Investigating pedestrian-level greenery in urban forms in a high-density city for urban planning

Authors: Junyi Hua[a], Meng Cai[b], Yuan Shi[c], Chao Ren[a,*], Jing Xie[a], Lamuel Chi Hay Chung[a], Yi Lu[d], Long Chen[d], Zhaowu Yu[e], Chris Webster[a]

[a] Faculty of Architecture, The University of Hong Kong, Hong Kong, China

[b] School of Architecture, The Chinese University of Hong Kong, Hong Kong, China

[c] Department of Geography & Planning, University of Liverpool, Liverpool, UK

[d] Department of Architecture and Civil Engineering, City University of Hong Kong, Hong Kong, China

[e] Department of Environmental Science and Engineering, Fudan University, Shanghai, China

E-mail addresses:

Junyi Hua: jhua@hku.hk

Meng Cai: caimeng@link.cuhk.edu.hk

Yuan Shi: yuan.shi@liverpool.ac.uk

Chao Ren: renchao@hku.hk

Jing Xie: xiej412@hku.hk

Lamuel Chi Hay Chung: lchchung@hku.hk

Yi Lu: yilu24@cityu.edu.hk

Long Chen: lochen6-c@my.cityu.edu.hk

Zhaowu Yu: zhaowu_yu@fudan.edu.cn

Chris Webster: cwebster@hku.hk

*Corresponding author:

Dr. Chao Ren

E-mail address: renchao@hku.hk

Postal address: 4/F, Knowles Building, Faculty of Architecture, The University of Hong Kong, Pokfulam, Hong Kong, China

Highlights

- A city-wide investigation on street greenery using Google Street View images and deep learning
- Estimated spatial variation in street greenery in Hong Kong
- Quantified greenery in different urban forms represented by LCZs
- Inconsistency between GSV greenery and NDVI varied across LCZs.
- The analytical approaches based on open-source data are transferable.

Investigating pedestrian-level greenery in urban forms in a high-density city for urban planning

Abstract

The understanding of pedestrian-level greenery across urban forms in built environment configurations in high-density cities is insufficient. We conducted a citywide investigation of urban greenery from the pedestrian perspective by developing a deep learning technique to extract greenery from fisheye images generated from Google Street View images in Hong Kong. Relying on open-source data, we compared pedestrian-level greenery measurements with the satellite-based normalized difference vegetation index (NDVI) in diverse urban forms represented by local climate zone classes. Street greenery was spatially variant, and low greenery was found predominantly in private residential and commercial/business lands in high-density areas. Pedestrian-level measurement and the NDVI were strongly correlated, but the inconsistency between them increased from high- and mid-rise forms to low-rise forms and from compact forms to open forms. We also demonstrated the idea of integrating nearby street greenery with spatial information on population and urban morphology for inequality analysis. Potential implications for urban planning are provided. The findings linking street greenery with urban morphology are useful for urban and greenery planning in climate-resilient, sustainable, and healthy cities. Our analytical approach using open-source data is transferable to other high-density cities.

Keywords: urban green space, street view image, deep learning, urban morphology, pedestrian level; local climate zone

1. Introduction

As a key component of the natural environment in cities, street greenery can be used as a sustainable, nature-based solution to provide multiple social and environmental benefits (Mullaney et al., 2015; Roy et al., 2012) for achieving sustainable development goals, particularly good health and well-being, climate adaptation, and sustainable cities and communities (Turner-Skoff & Cavender, 2019). Sustainable city development requires a close link between social and environmental dimensions (Bibri, 2018). Therefore,

the measurement of individuals' accessibility and exposure to urban greenery from the pedestrian perspective is crucial in urban planning (Fernandes et al., 2019; Ye et al., 2019). There is a growing trend in measuring the distribution of street greenery in urban areas by multiple techniques (Labib et al., 2020; Shahtahmassebi et al., 2021).

1.1. Approaches to measuring urban greenery

Multiple approaches quantitatively measure urban greenery. Small-scale investigations can use high-resolution data sources, such as on-site photography (Jiang et al., 2017; Yang et al., 2009) and LiDAR (MacFaden et al., 2012), which are generally used for specific purposes and highly depend on funding resources; however, for large, city-scale greenery measurements, satellite images and street view images are more suitable data sources. Both feature extensive datasets, allowing studies that measure greenery exposure in urban areas. Satellite images have long been used to measure greenery at different spatial scales from an overhead perspective by creating specific indices, such as the widely adopted normalized difference vegetation index (NDVI), as a measure of greenness or density of vegetation on a patch (Shahtahmassebi et al., 2021). Street view images, represented by Google Street View (GSV), are increasingly used to explore innovative approaches for extracting and evaluating city-scale street-level environments in urban areas (Li et al., 2018; Middel et al., 2019; Rundle et al., 2011; Seiferling et al., 2017). Alternative street view products provided by Tencent Maps and Baidu Maps in China, Yandex Maps in Russia, and Mapillary have also been used to measure urban environments (Kang et al., 2020; Neuhold et al., 2017). Based on on-site photographs in different directions at street intersections (Yang et al., 2009), an index was created after modification in combination with GSV images to measure visible street greenery (Li et al., 2015). Street view images capture the vertical dimension of urban environments (Middel et al., 2019), namely, green façades or shrubs under canopies; pedestrians can see and perceive from the ground in the street. Satellite imagery collects the canopy area and green roofs or green spaces behind buildings from a bird's-eye view. The difference in perspectives causes inconsistencies in the measurements.

The tree view factor (TVF), derived from the sky view factor (Oke, 1981; Steyn, 1980), has been widely used to portray urban outdoor environments and innovatively capture the three-dimensional form of greenery canopy in a photography-based fisheye image (Gong et al., 2018; Liang et al., 2020). Fisheye images, initially used for projecting the radiating environment (Steyn, 1980), depict urban environments perceived by pedestrians within an entire radiation space. Street greenery characterized by the TVF can therefore reflect how pedestrians benefit from street greenery's regulating ecosystem services, such as microclimatic amelioration that depends on shading and evapotranspiration (Richards & Edwards, 2017). GSV images facilitate the creation of large datasets of fisheye images for computing the view factors and therefore have been increasingly used for that aim (Carrasco-Hernandez et al., 2015; Li et al., 2018; Middel et al., 2018).

1.2. Inconsistency between satellite-derived vegetation indices and street view image-based greenery measurements

A research trend is to examine inconsistencies between satellite-derived vegetation indices and street view image-based greenery measurements to provide evidence for urban planning (Helbich et al., 2019; Kumakoshi et al., 2020; Larkin & Hystad, 2019; Tong et al., 2020; Villeneuve et al., 2018; Ye et al., 2019). In studies of Singapore and Hong Kong, GSV-based greenery measurement and the NDVI were only moderately correlated (Lu et al., 2019; Ye et al., 2019). In a case study of Nanjing, Tong et al. (2020) discovered variations in the association between street view-based greenery measurements and the NDVI across urban functional zone types. Lu et al. (2019) identified three neighborhood patterns in Hong Kong based on the relationship between the NDVI and GSV-based measurements. This mismatch suggests that satellite image-based measurements may over- or under-estimate the actual personal exposure to urban greenery because of differences in perspective (Larkin & Hystad, 2019). Therefore, in urban planning, merely considering vegetation cover from an overhead perspective, which is a common method, may lead to biases in measuring the pedestrian environment of greenery. Measurements based on street view images could better reflect pedestrians' exposure to greenery on the street than overhead views and could

therefore represent its impacts on physical activity in the public domain (Lu, 2019) and public health (Kang et al., 2020).

1.3. Effects of urban forms

Urban forms, widely considered in urban climate research and urban planning (Middel et al., 2019; Xu et al., 2017), may affect the inconsistency between street view-based greenery measurements and satellite-derived indices. Urban environmental studies that provide evidence for urban planning, particularly greening master plans, focus on both urban natural landscape components and built environments that interact with each other. The characteristics of urban greenery embedded in different built environments may be detected from different perspectives. Exposure to greenery depends on both the provision of greenery and other built environment attributes such as building density, community forms, and street characteristics (Davies et al., 2008; Pham et al., 2017; Zhang et al., 2020). Mixed urban forms have mixed effects on greenery investigations and greenery exposure. The mismatch between the two measurements may vary across urban forms in complex high-density urban contexts because the detection of urban greenery from both pedestrian and overhead perspectives would be affected by the configuration of surrounding buildings. Exploring the mismatch will not only help understand the current situation of urban greenery in different urban forms but also inform future urban planning and greenery design to improve pedestrian exposure to greenery in different urban settings instead of merely increasing vegetation cover. However, according to our review of the literature, how street view-based pedestrian-level greenery measurements and satellite-derived vegetation metrics are inconsistent in diverse urban forms has not been studied.

1.4. Local climate zone (LCZ) classification

A standardized scheme called the LCZ classification system allows fine-scale spatial investigation of the effects of 3-D urban morphology on street greenery measurements. The LCZ scheme (**Fig.** [1]), developed

[1]**Fig.** in Supplementary Materials shows the LCZ typology based on Stewart and Oke (2012). It was created by Demuzere et al. (2020), derived from https://www.wudapt.org/lcz-resources/.

by Stewart and Oke (2012), categorizes urban surface structures and covers ten built types and seven natural types with different climatic responses. The built types were differentiated in building height, density, and arrangement of trees. Because of its detailed description of 3-D urban morphology (Demuzere et al., 2020) and across-city consistency as an internationally accepted standard, the scheme has recently gained increasing applications in research on UHIs (Lehnert et al., 2021; Xue et al., 2020) and urban landscape planning (Liu et al., 2020; Zhao et al., 2020). The LCZ classification provides a new perspective for understanding pedestrian-level street greenery~~, spatial variation in street greenery, and differences between pedestrian level greenery and overhead view vegetation cover~~ across 3-D urban forms in high-density urban contexts. Different greening strategies can be formulated and implemented in various urban forms. In addition, LCZ classification is an international standard, and the properties and details of each built class must be defined by local situations. Although some LCZ classes are defined by the presence of vegetation, detailed information on vegetation characteristics of the built LCZ types remains limited (Bartesaghi-Koc et al., 2019); thus, fine-scale quantification is necessary.

1.5. Inequality in urban greenery

Inequalities in urban greenspace provision have drawn increasing attention and have been widely observed from spatial and socioeconomic perspectives (Ahn et al., 2020; Kabisch & Haase, 2014; Wolch et al., 2014). Inequality implies that in addition to supply, demand should be considered. The investigation of visual exposure to street-level urban greenery needs to consider the distribution of end users. More importantly, urban morphology may aggravate inequality but is evidence of greenery planning. The demand for outdoor greenery may be greater for residents in high-density high-rise areas, where the space for greening is limited, than that for residents in open areas. Specific groups of individuals, such as elderly individuals, are more vulnerable to environmental stresses, such as extreme heat (Åström et al., 2011) and heavy air pollution (Yang et al., 2018), and supply-demand analysis requires consideration of sub-populations and totals (Kabisch et al., 2017). According to our review of the literature, no studies have combined street view image-based greenery measurements with both urban

morphology information and population and subpopulation distributions to address inequalities in urban greenery provision. This research gap prompted us to establish a link to facilitate future urban planning.

1.6. Research objectives

In this study, our objective was to deepen the GSV image-based investigation of pedestrian-level street greenery in complex urban forms in high-density cities by using open-source data. We conducted a case study in Hong Kong and developed a pedestrian-level street greenery indicator based on fisheye images created from GSV images. Specifically, this study aimed to (1) measure citywide pedestrian-level street greenery, (2) quantify greenery and the relationship between the indicator and the NDVI in different urban forms, and (3) explore how to use the GSV-based approach in street greenery inequity analysis. Our study is the first to quantify greenery captured from streets in different urban forms; thus, it is a pioneering attempt to account for the effect of urban morphology on greenery measurements. The research findings are expected to help the understanding of street greenery from a pedestrian perspective and provide potential implications for urban greenery planning in high-density urban contexts.

2. Methods

2.1. Study area

The study was conducted in Hong Kong, a subtropical, high-density city on the southern coast of China (**Fig. 1**). The city covers an area of 1111 km^2, much of which is hilly and mountainous. It accommodates approximately 7.5 million people on approximately 25% of the land (PlanD, 2020b). The city comprises 18 districts: four on Hong Kong Island, five in Kowloon, and nine in the New Territories. The old urban areas are concentrated on the northern coast of Hong Kong and Kowloon. High-density urban areas are filled with compact high-rise buildings and deep street canyons (Zheng et al., 2018). Despite the approximately 440 km^2 area of country parks and special areas, green space in built-up areas is generally regarded as insufficient. The current average area of open space provision per capita in old urban areas and new towns is less than 3 m^2, far below that of neighboring large Asian cities (Jim & Chan, 2016). The

figure in old compact areas, such as Mong Kok in Kowloon, is even smaller than the low local standard, which, given the population density, represents a serious green space inequality problem (Lai, 2017). Extensive impervious surfaces further contribute to an extremely low amount of street greenery (Jim & Chan, 2016). The Hong Kong government has implemented a Greening Master Plan for green urban areas and new towns since 2004 (CEDD, 2020). The aim of the 2015 document "Hong Kong 2030+: Towards a Planning Vision and Strategy Transcending 2030" was to achieve a livable high-density city (PlanD, 2016).

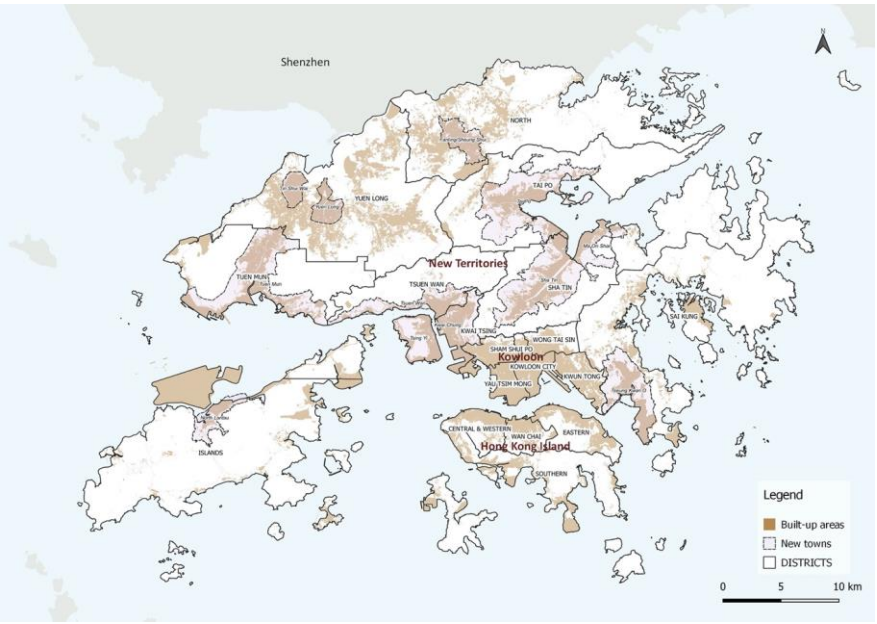

Fig. 1. Map of the study area, Hong Kong. (Built-up areas are based on the spatial information of land utilization for 2019 released by the Planning Department.)

2.2. Data sources

2.2.1. GSV data

As discussed in the prior section, GSV is an increasingly well-used image source for analyzing street-level urban greenery. To investigate the spatial distribution of street greenery in Hong Kong, we collected GSV images taken annually in 2019 and 2020 at approximately 53,000 locations every 50 m along the more than 2000 km road network of the city via the Street View Static API. For each geolocation, eight images, which had a 120° horizontal field of view, the maximum value allowed, and covered the 360 °horizontal circle from four directions (left, right, front, and back), and two vertical angles were stitched to a panorama. Locations in tunnels and highways were excluded. Hence, approximately 37,000 panoramic images were used for analysis. Detailed information on GSV collection is presented in the Supplementary Material. **Fig. 2** shows an example of the composite GSV images and processed panorama for one point.

(a)

(b)

Fig. 2. GSV image collection and processing at a point: (a) eight images captured from four directions and two angles and (b) panorama

2.2.2. LCZ classification

An LCZ map (**Fig. 3**) of Hong Kong was derived from the LCZ map of the Pearl River Delta (PRD) region for the year 2019 at a resolution of 100 m, created by using the suggested workflow in Chung et al. (2021). The map presents the detailed urban surface morphology of Hong Kong. The workflow used open-source remote sensing imagery from Jan 1, 2019, to Dec 31, 2019, the cloud computation platform Google Earth Engine (GEE), and the machine learning classifier random forest (Breiman, 2001; Pal, 2005). Eighteen LCZ classes were identified: the 17 classes defined by Stewart and Oke (2012) and the World Urban Database and Access Portal Tools, and an additional class LCZ H for wetlands, which are

common in the PRD region. The built-up areas of Hong Kong were categorized into LCZs 1–10 by the 3-D urban surface morphology. LCZs 1–6 are the main classes of built-up areas and differ in the density and height of the buildings. Building density was categorized as open and compact. Building heights were categorized as low-rise, mid-rise, and high-rise. A table of the classified LCZ properties and a confusion matrix of the classification accuracy are available in the Supplementary Material (Tables S1 and S2). The confusion matrix summarizes the producer and user accuracies of each LCZ type obtained from the classification based on the elite variable combination in Chung et al. (2021). The overall accuracy (76.1%), built-up (LCZ 1-10) accuracy (73.4%), natural land (LCZ A-H) accuracy (71.6%), and Kappa (0.747) showed that the classification achieved high classification accuracies.

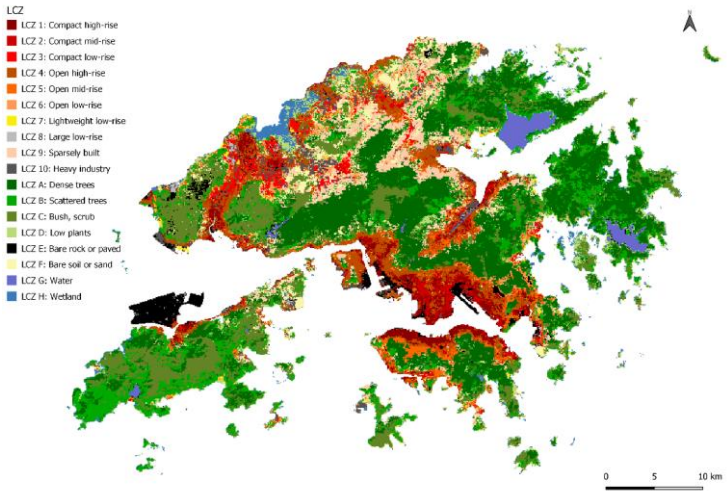

Fig. 3. Local climate zone map of Hong Kong based on Chung et al. (2021)

2.2.3. Other data sources

The NDVI captures the earth-view greenness of vegetation cover. Sentinel-2 MSI Level-2A imagery was used to calculate the NDVI. Detailed information on the data source and calculation is presented in the Supplementary Material. The NDVI ranges from -1 to 1. Because the photography period of the GSV

images covered 1 year from 2019 to 2020 (approximately 72% from May 2019 to Nov 2019) and vegetation in Hong Kong in a subtropical region is primarily evergreen, we calculated the average value of full-year NDVI in 2020 from January 1 to December 31 to identify the vegetation cover in the study area.

Information on land utilization is from open access sources from the Planning Department (PlanD, 2020b). The land utilization of the whole territory of Hong Kong covers 10 built or natural classes and 27 specific categories. A raster map at a spatial resolution of 10 m for 2019 was derived for this study.

The 100 m resolution gridded estimates of the entire population and the male and female population in each age group in Hong Kong for 2020 were freely collected from WorldPop (www.worldpop.org). The elderly population was calculated as the sum of the estimates for the groups aged 65 years and above (Bondarenko et al., 2020).

All data used in the study, including the GSV images, remote sensing data for LCZ classification and NDVI calculation, local land utilization, and gridded population, were derived from open sources, making our method highly replicable.

2.3. Green view factor estimates

2.3.1. Greenery extraction using deep learning and validation

We applied a deep learning technique to panoramic images to extract greenery information. Semantic segmentation with deep learning has proven effective in pattern recognition and is a state-of-the-art, powerful tool for extracting information from images (Hesamian et al., 2019). Based on a pre-trained network, objects in the panorama images were classified into 32 predefined classes and further categorized into three main classes: vegetation, urban, and sky. The vegetation class captures all vegetation, including trees and other greenery; the urban class covers objects other than greenery and sky. The accuracy of the vegetation classification was 95%. Furthermore, the segmented panorama images were transformed to a complete 180° fisheye sky view image, using the panorama tools developed by

Dersch (2005). The workflow of vegetation extraction is summarized in **Fig. 4**, and details of the extraction process are presented in the Supplementary Material. Semantic segmentation and accuracy assessments were performed on MATLAB 2020b.

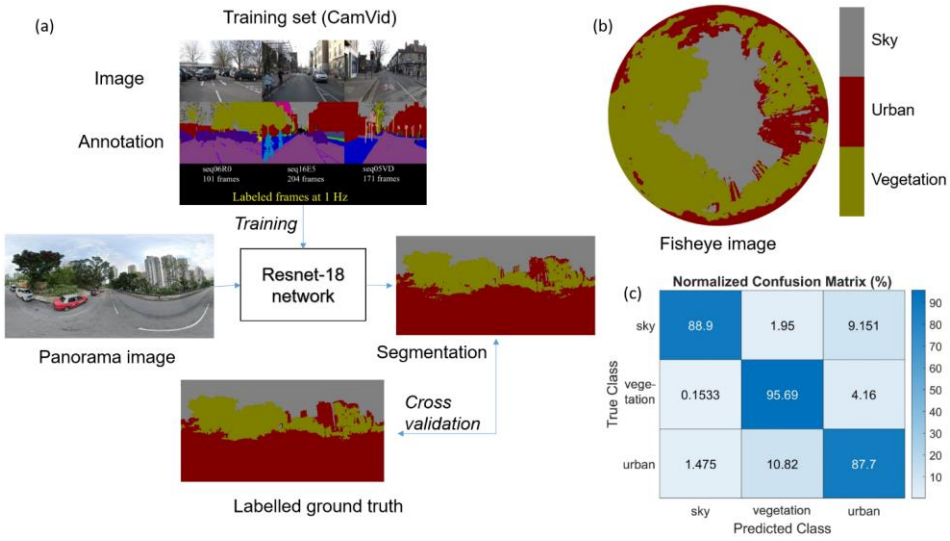

Fig. 4. Greenery extraction using deep learning: (a) workflow of semantic segmentation and validation, (b) transformation to fisheye image, (c) confusion matrix

2.3.2. Green view factor (GVF) calculation

In this study, we defined a GVF as the ratio of all visible greenery at a certain point to the overlying hemisphere based on the TVF. The GSV fisheye images were categorized into three classes: vegetation, urban, and sky. The GVF quantifies the proportion of the vegetation class in the fisheye image and theoretically ranges from 0 to 1. Therefore, GVF was computed using the following equation:

$$GVF_i = \frac{VegetationPixel_i}{P},$$

where for the GSV image i, $(i = 1\ to\ n)$, $VegetationPixel_i$ denotes the number of pixels of the vegetation class, and P is the total number of pixels constituting fisheye image i (1080 × 1080 in this study).

2.4. Data analysis

Point-based GVF was mapped in the road network across the built-up areas of Hong Kong to visualize the distribution of street-level urban greenery. The GVF data were divided into five categories from low to high, based on the Jenks natural break classification method. This method was used to decrease within-class variance and maximize between-class variance. We probed the differences in street greenery measured by the GVF across 18 districts, 12 new towns, 9 principal land use types in built-up areas, and 18 LCZ classes based on GVF statistics. The land use of each point was determined by the dominant land use (the largest proportion, except for roads and transportation facilities) within a 300 m buffer of the point.

The relationship between the GVF and NDVI was then estimated for each GSV point. Spearman's rank-order correlation was computed between the GVF and the mean NDVI within buffers at different distances (10 m, 20 m, 50 m, and 100 m) from the GVF points, according to Lu et al. (2019) and Ye et al. (2019) and Hong Kong's road width. For the 10 m resolution NDVI raster map, values below zero represented non-vegetated areas and were therefore reassigned to zero. The distance with the highest correlation was selected for subsequent analysis. We assumed that the 20 m buffer may be the most appropriate to measure the mean NDVI for the following point-scale analysis because most roads in urban areas are designed to be less than 15 m wide (PlanD, 2021), and the 20 m buffer can best capture greenery on paths along the side of roads.

To explore the effect of urban morphology, we estimated Spearman's correlation between the two metrics for each LCZ class. The focus was the common classes in built-up areas, LCZs 1–6, characterized by different compactness and heights of buildings. The correlation between the GVF and NDVI was estimated at both scales of the GSV and LCZ grids. The point-scale analysis used the points' GVF and

mean NDVI within the best buffer distance, as aforementioned. For the grid-scale estimation, the point-based GVF and the 10 m resolution NDVI were joined as mean values into the 100 m resolution LCZ grids through spatial join and zonal statistics, respectively, in QGIS 3.16. Only LCZ grids covered by GSV points were included. For both the point and grid data, we conducted regression analysis to determine the linear relationship between the GVF and mean NDVI using Stata 16.1.

Last, the GVF and population density were combined to visualize the exposure to surrounding street greenery at the LCZ scale. Point-based GVF was joined as mean values into the 100 m resolution LCZ grids. Next, we analyzed the walking accessibility of greenery in daily life: the average of the mean GVF for the (25) grids within the 500 m × 500 m zone as a buffer defined by each LCZ grid was calculated to reflect the surrounding street greenery within and around each LCZ grid within a short walking distance according to local standards and the literature. The Hong Kong Planning Standards and Guidelines stipulates that a local open space should preferably be within 400 m of residences (PlanD, 2020a). The buffering approach is frequently used to measure the accessibility of or exposure to green spaces, and a distance of 300 m is a common threshold (Ekkel & de Vries, 2017; Labib et al., 2020). The mean of the entire population and elderly population (aged 65 years or above) were summarized into the 100 m resolution LCZ grids through the zonal statistics of the 100 m resolution maps derived from WorldPop. The mean surrounding street greenery and population were divided into five and three categories, from low to high, respectively, based on the Jenks natural breaks classification method. Thus, we characterized each grid in three aspects: surrounding street greenery, population density, and LCZ. The overall workflow of the methodology is shown in **Fig. 5**.

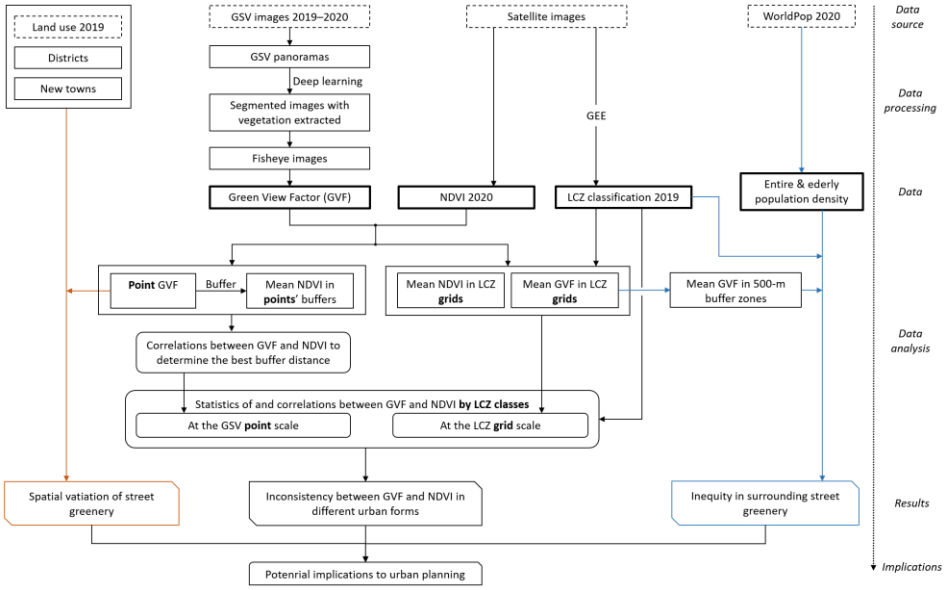

Fig. 5. Flowchart of the methodology

3. Results

3.1. Street greenery distribution based on the green view factor

The GSV point-based GVF map is presented in **Fig. 6** to show the citywide street greenery distribution, classified as Jenks natural breaks, particularly the distribution in the old urban areas in Kowloon and the northern coast of Hong Kong Island. Overall mean and median values of point-based GVF are 0.39 (±0.24) and 0.36, respectively, which are close to the corresponding values of LCZ grid-based GVF. Citywide street greenery has been found to vary spatially. Low degrees of greenery were mainly concentrated in the old urban areas (**Fig. 6b)** and the central areas in some new towns; highly green areas were mainly at the Peak, atop Victoria Peak, on Hong Kong Island, and scattered on the peripheries of the urban areas. The overall street greenery distribution is consistent with the NDVI map shown in **Fig. 7**. The map of the LCZ grid-scale GVF is presented in the Supplementary Material (**Fig. S2**) for reference.

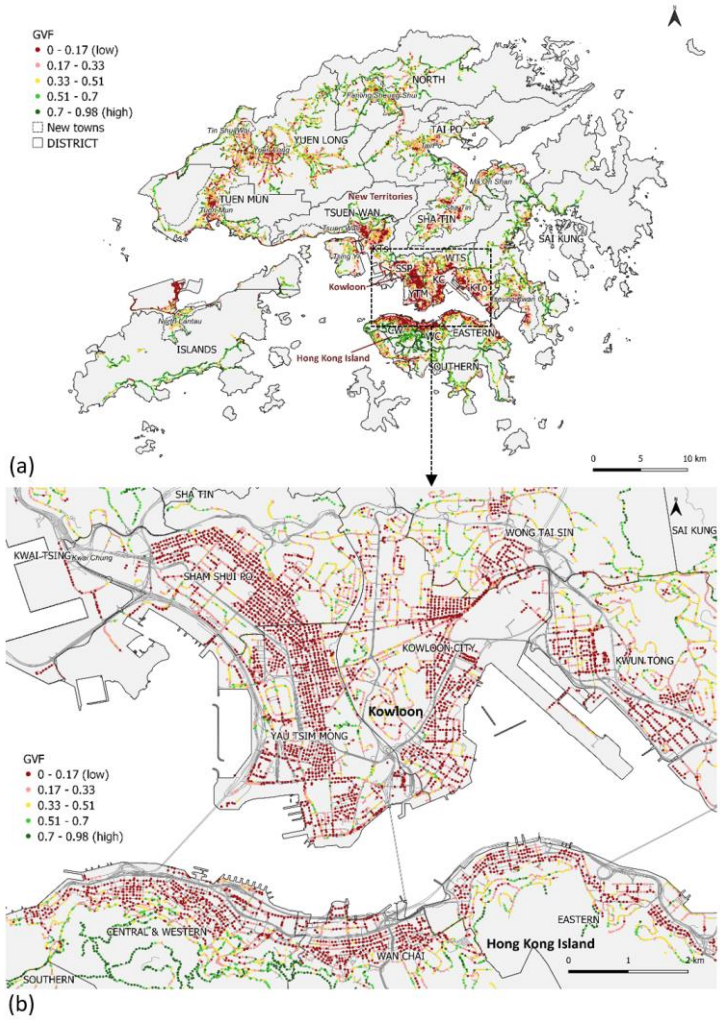

Fig. 6. Maps of point-based GVF of (a) the whole city and (b) the old urban areas in Kowloon and the northern part of Hong Kong Island

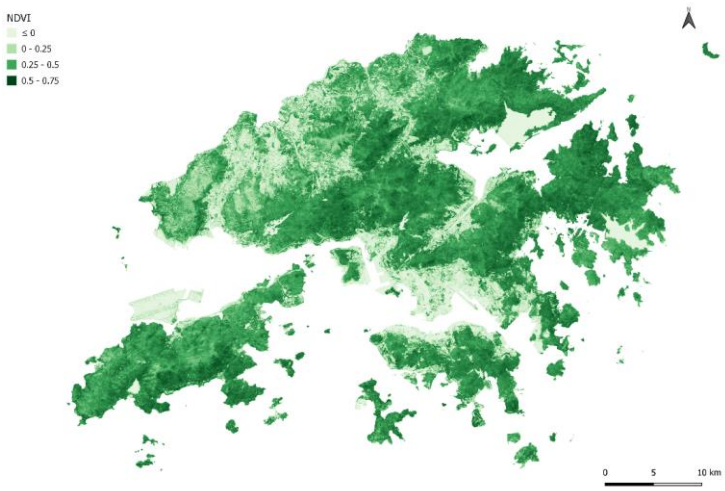

Fig. 7. NDVI map of Hong Kong

Street greenery in each district, new town, land utilization type, and LCZ class are depicted in violin plots (**Fig. 8.**). Variations across districts further support the overall distribution that was summarized. The median GVF values in the four districts of Hong Kong Island were between 0.30 and 0.47. Except for the Southern District, all show the presence of peaks at low GVF, reflecting the low greenery on the northern coast of Hong Kong Island. The central, western, and Wan Chai areas also had peaks of high values on the peripheries of urban areas, as aforementioned. All five districts in Kowloon show a comparatively low median GVF, particularly in Yau Tsim Mong (0.11), Sham Shui Po (0.15), and Kowloon City (0.17), where the lowest degrees of street greenery in Hong Kong were found. The low-greenery areas correspond to the dense street networks in these districts in the old urban area (**Fig. 6b)**. In the New Territories, the average street greenery across districts ranges from 0.29 in Kwai Tsing to 0.49 in North, much better than that in Kowloon.

Because the built-up areas of the New Territories are found across urban, suburban, and rural conditions, statistics of the GVF in 12 new towns will help to understand spatial variation in street greenery in the

urban areas of the New Territories[2]. The median GVF for all 12 new towns is 0.35. The lowest median values of the GVF are found in several early-developed new towns, such as Yuen Long (0.24), Kwai Chung (0.27), and Tsuen Wan (0.29), and the highest value is 0.48 in North Lantau, the newest new town. Furthermore, the shapes of the GVF distributions within new towns also varied.

The distribution of street greenery is disproportionate across the types of land use. Land for private residential and commercial/business and office has a comparatively low median GVF (approximately 0.2 and 0.1, respectively), with peaks at approximately 0.1. Lands for public residential, rural settlement, government, institutional and community facilities, and open space and recreation shared a similar distribution and degree of street greenery, with a median GVF over 0.3. Street greenery on land intended for industrial use varies across industrial activities. Lands for warehouse and open storage and industrial lands ranked at the top and bottom, respectively, among the nine land use types.

Variations in street greenery distribution were found among the LCZ classes. LCZs 1 and 2 (compact high-rise and mid-rise), mainly concentrated in old urban areas, have the lowest GVF median values at 0.18 and 0.17, respectively; the situation was slightly better in compact low-rise areas (0.23) and much greener in open LCZs (0.41–0.47). Street greenery in 'natural type' LCZs is notably higher than that in built types and decreases from dense-tree LCZs (0.75) to low plant LCZs (0.51).

[2] Titles of some new towns are the same as titles of some districts, but the boundaries differ. These new towns are newly developed parts mainly for housing within the corresponding districts. Boundaries of districts and new towns are shown in **Fig. 1**.

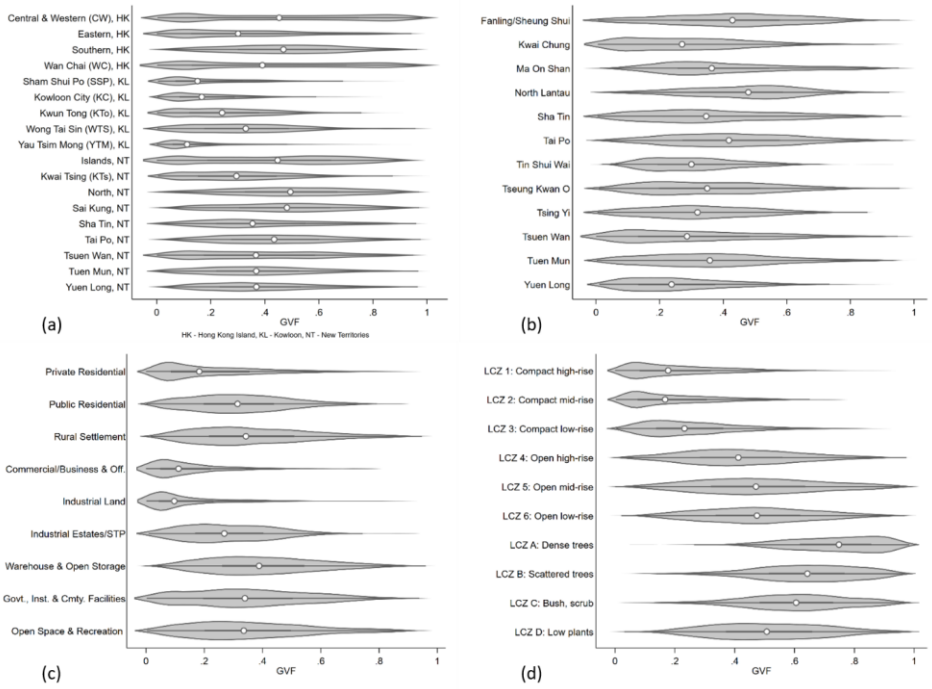

Fig. 8. Violin plots of the GVF by (a) district, (b) new town, (c) land utilization type, and (d) LCZ class

3.2. Comparison of street greenery (GVF) and vegetation cover (NDVI) by LCZs

Pedestrian-level greenery and remotely sensed vegetation were strongly correlated at the scales of GSV and LCZ grids across the city. At the point scale, the correlation decreased with the buffer distance used to measure the mean NDVI. Spearman's ρs for GVF versus the mean NDVI within 10 m, 20 m, 50 m, and 100 m buffers of the GVF points are 0.81 ($p < 0.001$), 0.83 ($p < 0.001$), 0.80 ($p < 0.001$), and 0.75 ($p < 0.001$), respectively. The highest correlation of the 20 m buffer supports our assumption of the use the 20 m buffer to measure the mean NDVI for the subsequent point-scale analysis. At the grid scale, Spearman's correlation coefficient (Spearman's ρ) was 0.77 ($p < 0.001$).

The statistics for the GVF, NDVI, and correlations between them by LCZs for GSV points and LCZ grids are presented in Table 1. We focused on the main built-type LCZs (1–6), which dominate built-up areas. The GSV points sampled in LCZs 1–6 accounted for 83.9% of all points in the built-type LCZs (1–10). The sampling was representative because LCZs 1–6 accounted for 82.9% of the LCZs 1–10 covered by GSV points. The statistics of the GVF points in Table 1 are also shown in violin plot (d) in Fig. 8. Overall, the variation trends of the GVF and NDVI across the LCZ classes were consistent between the point and grid data. Wilcoxon rank sum tests show that the distributions of the GVF and NDVI significantly differed between compact LCZs (1–3) and open LCZs (4–6), between low-rise LCZs (3 and 6) and high- and mid-rise LCZs (1, 2, 4, and 5), and between built types (LCZs 1–10) and vegetated LCZs (A–D) for both the grid and point data series. The test results are presented in the Supplementary Material (Table S3).

Linear relationships were found between the GVF and NDVI for point data (GVF = 1.124 × NDVI + 0.113, r^2 = 0.664) and grid data (GVF = 0.993 × NDVI + 0.136, r^2 = 0.582). Similar relationships were also found in LCZs 1–6. Scatter plots of the GVF and NDVI for the point data by LCZ class are shown in **Error! Reference source not found.**. The points of the low GVF and NDVI were mainly in LCZs 1 and 2. Extremely low greenery was observed in LCZs 1 and 2. Among the points in LCZs 1 and 2, 5.3% and 2.4% had a zero mean NDVI within 20 m buffers, respectively, and 17.8% and 15.9% had a mean NDVI below 0.01, which means nearly no vegetation. However, most of the near-zero NDVI points had GVF values that were not close to zero.

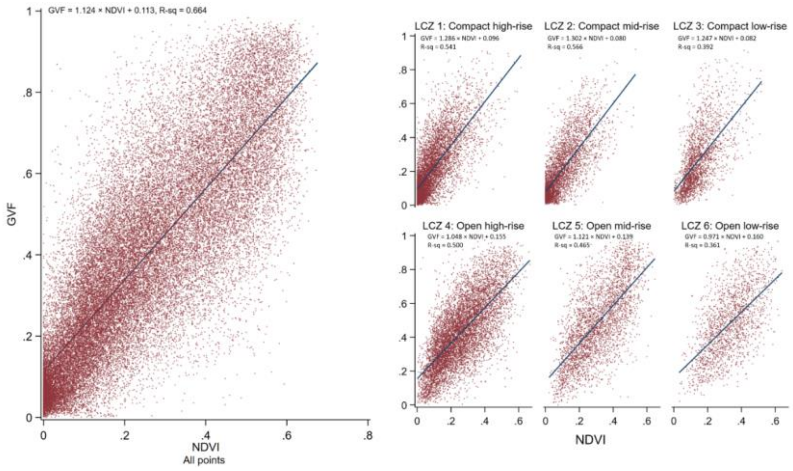

Fig. 9. Scatter plots of the GVF and NDVI at the point scale by LCZ classes

Spearman's correlation varied across the LCZ classes for both points and grids. Overall, the correlation for the built-type LCZs (1–10) was notably higher than that for the vegetated LCZs (A–D). For LCZs 1–6, Spearman's ρs for compact LCZs (1–3, 0.74 and 0.67, respectively, for points and grids, with p values < 0.001) are greater than those for open LCZs (4–6, 0.69, and 0.53, respectively, with p values < 0.001). Regarding building height, correlations for high-rise LCZs (1 and 4) at 0.81 and 0.74 and mid-rise LCZs (2 and 5) at 0.84 and 0.78 with p values < 0.001 are greater than those for low-rise LCZs (3 and 6) at 0.74 and 0.64 with p values < 0.001. Compact, high- and mid-rise LCZs (1 and 2) show strong correlations (approx. 0.75 for points and 0.7 for grids with p values < 0.001), followed by open, high- and mid-rise LCZs (4 and 5) with strong correlations for points (approx. 0.7 with p values < 0.001) but moderate correlations (over 0.5 with p values < 0.001) for grids. Low-rise LCZs had even lower correlations, especially weak-moderate for grids (0.44 and 0.38 with p values < 0.001). Moreover, correlations and variations in correlations for grid data are greater than those for point data. For LCZs A–D, the class of dense trees exhibited weak correlations, particularly at the grid scale (0.11, p = 0.0024).

3.3. Application to investigating inequity in street greenery

Street greenery assessed by the point-based GVF and the entire population within a 500 m buffer of points were moderately and negatively correlated (Spearman's $\rho = -0.44$, $p < 0.001$). A comparable correlation (Spearman's $\rho = -0.35$, $p < 0.001$) was found between area-averaged street greenery within 500 m × 500 m zones and the entire population in the central LCZ grid. The negative correlation with the elderly population was similar ($\rho = -0.32$, $p < 0.001$).

Error! Reference source not found. presents a map of the surrounding street greenery for the old urban areas of Hong Kong in 100 m resolution grids of LCZs, together with the boundaries of the tertiary planning units (TPUs) and maps of GVF, road network, population density, and LCZs for a specific central area in Kowloon. The Planning Department divided the territory of the city into 291 TPUs for spatial planning. **Error! Reference source not found.a** shows that the surrounding street greenery within buffer zones is also spatially variant, and the lowest degree of surrounding street greenery is concentrated in several connected areas in the old urban areas. **Error! Reference source not found.b** shows the central part of the Kowloon Peninsula. The population density can be interpreted as the number of people in a 100 m × 100 m grid equivalent to 100 times per square kilometer. Because the entire population density is highly correlated with the elderly population density, the map for the elderly population is presented in the Supplementary Material (**Fig. S3**). TPUs vary in urban morphology, road networks, population density, and surrounding street greenery. Residents in moderately densely populated open LCZs had higher exposure to greenery, for example, in TPU 226. TPU 221 has a compact high- and mid-rise urban morphology, high population density, dense road networks, and low street greenery exposure. In TPU 236, LCZ classes and population density varied, but street greenery was relatively low.

Table 1 Statistics of the GVF and NDVI by LCZs

	Points								LCZ grids							
			GVF			NDVI					GVF			NDVI		
LCZ	Obs.	Corr.	Median	Mean	SD	Median	Mean	SD	Obs.	Corr.	Median	Mean	SD	Median	Mean	SD
Overall	37813	0.83	0.36	0.39	0.24	0.22	0.24	0.17	19296	0.77	0.38	0.40	0.23	0.24	0.27	0.17
LCZ 1: Compact high-rise	6507	0.75	0.18	0.22	0.17	0.07	0.10	0.10	3094	0.70	0.19	0.22	0.16	0.08	0.10	0.08
LCZ 2: Compact mid-rise	3865	0.76	0.17	0.21	0.16	0.07	0.10	0.09	1784	0.71	0.19	0.22	0.15	0.09	0.11	0.08
LCZ 3: Compact low-rise	2239	0.64	0.23	0.27	0.17	0.13	0.15	0.09	1194	0.44	0.25	0.27	0.16	0.14	0.14	0.06
LCZ 4: Open high-rise	7845	0.70	0.41	0.43	0.19	0.25	0.26	0.13	4030	0.55	0.42	0.43	0.18	0.27	0.28	0.13
LCZ 5: Open mid-rise	3234	0.68	0.47	0.48	0.21	0.30	0.31	0.13	1612	0.51	0.47	0.48	0.19	0.31	0.32	0.11
LCZ 6: Open low-rise	1763	0.59	0.47	0.48	0.19	0.33	0.33	0.12	940	0.38	0.48	0.48	0.18	0.34	0.35	0.10
LCZ 7: Lightweight low-rise	534	0.63	0.36	0.37	0.19	0.22	0.24	0.12	291	0.47	0.36	0.37	0.18	0.23	0.23	0.10
LCZ 8: Large low-rise	186	0.74	0.23	0.26	0.17	0.11	0.11	0.08	104	0.45	0.24	0.26	0.16	0.08	0.10	0.06
LCZ 9: Sparsely built	1814	0.63	0.57	0.56	0.20	0.41	0.40	0.13	1039	0.52	0.56	0.55	0.19	0.43	0.42	0.11
LCZ 10: Heavy industry	2360	0.69	0.32	0.35	0.19	0.20	0.21	0.12	1183	0.53	0.34	0.35	0.18	0.20	0.21	0.10
LCZ A: Dense trees	1353	0.32	0.75	0.73	0.15	0.54	0.53	0.07	765	0.11	0.73	0.72	0.14	0.56	0.55	0.06
LCZ B: Scattered trees	1872	0.53	0.64	0.63	0.18	0.50	0.48	0.10	1069	0.34	0.65	0.64	0.16	0.53	0.51	0.09
LCZ C: Bush, scrub	957	0.51	0.61	0.60	0.18	0.49	0.47	0.10	557	0.32	0.60	0.59	0.17	0.51	0.51	0.08
LCZ D: Low plants	713	0.52	0.51	0.52	0.19	0.41	0.39	0.12	396	0.42	0.53	0.53	0.18	0.41	0.41	0.11
LCZ E: Bare rock or paved	1384	0.53	0.16	0.19	0.14	0.09	0.10	0.08	620	0.48	0.17	0.19	0.13	0.09	0.10	0.07
LCZ F: Bare soil or sand	852	0.56	0.60	0.58	0.22	0.44	0.42	0.11	465	0.42	0.61	0.58	0.20	0.46	0.44	0.10
LCZ G: Water	12	0.70	0.02	0.23	0.33	0.10	0.12	0.12	1	.	0.52	0.52	.	0.11	0.11	.
LCZ H: Wetland	323	0.64	0.49	0.49	0.20	0.36	0.34	0.15	152	0.59	0.51	0.50	0.18	0.37	0.34	0.16
Compact (LCZs 1, 2, 3)	12611	0.74	0.18	0.22	0.17	0.08	0.11	0.10	6072	0.67	0.20	0.23	0.16	0.10	0.11	0.08
Open (LCZs 4, 5, 6)	12842	0.69	0.43	0.45	0.20	0.27	0.28	0.13	6582	0.53	0.44	0.45	0.18	0.29	0.30	0.12
High-rise (LCZs 1, 4)	14352	0.81	0.31	0.33	0.21	0.16	0.19	0.14	7124	0.74	0.33	0.34	0.20	0.18	0.20	0.14
Mid-rise (LCZs 2, 5)	7099	0.84	0.30	0.33	0.23	0.17	0.19	0.15	3396	0.78	0.31	0.34	0.22	0.19	0.21	0.14
Low-rise (LCZs 3, 6)	4002	0.74	0.33	0.36	0.21	0.20	0.23	0.14	2134	0.64	0.35	0.37	0.20	0.21	0.23	0.13
Built (LCZs 1–10)	30347	0.80	0.33	0.35	0.22	0.18	0.21	0.15	15271	0.73	0.34	0.36	0.21	0.20	0.22	0.15
Vegetated (LCZs A–D)	4895	0.55	0.65	0.64	0.19	0.50	0.48	0.11	2787	0.39	0.65	0.64	0.17	0.53	0.51	0.09

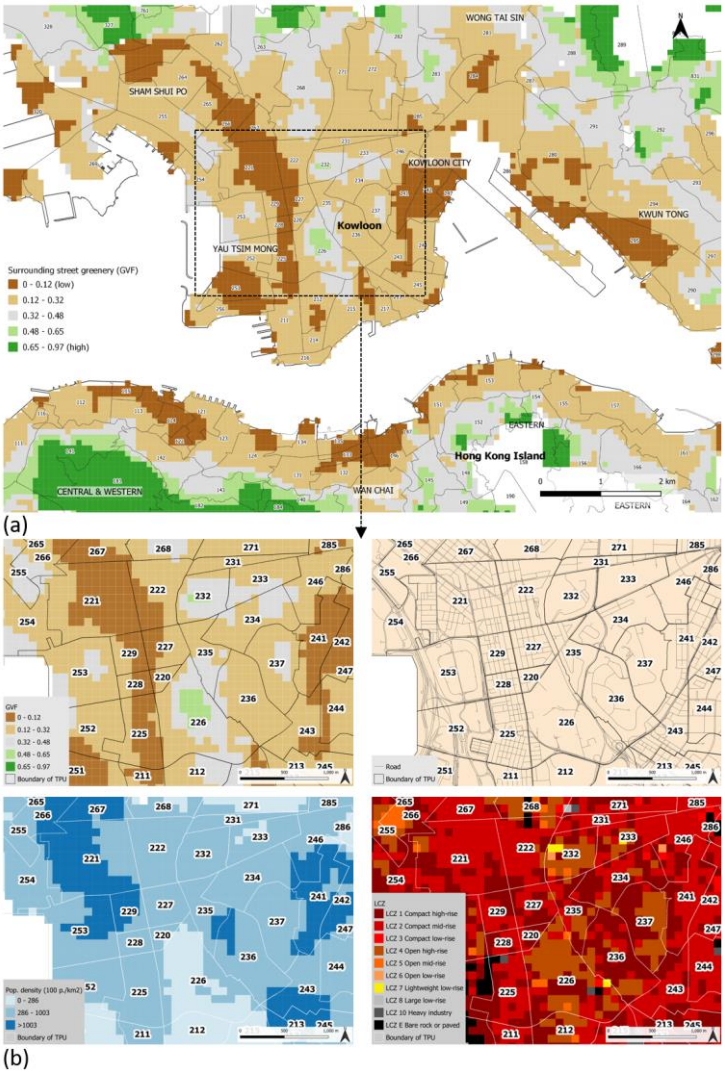

Fig. 10. Surrounding street greenery at the scale of LCZ grids in the old urban areas (a) and a central part of Kowloon Peninsula with information on GVF, road network, population density, and LCZs (b)

4. Discussion

4.1. Spatial variation in street greenery

There is marked spatial disparity in visible street greenery across built-up areas in Hong Kong. Greenery is generally insufficient in high-density urban areas (Haaland & van den Bosch, 2015). Old urban areas in Kowloon and the northern coast of Hong Kong Island have long been developed and dominated by compact high- and mid-rise buildings with dense and narrow streets. There is limited space along streets for greenery, except for inset urban parks and pocket gardens. The worst situation is in areas in Kowloon and is aggravated by the situation of residents with a low income. For instance, in Yau Tsim Mong, Sham Shui Po, and Kowloon City, residents with a low income can only afford housing in crowded, densely distributed old buildings. The disparity is more apparent when comparing the in-district variance on the northern coast of Hong Kong. Low street greenery is found in compact areas of Wan Chai and central, where private residential and commercial/business buildings are mixed in LCZs 1 and 2, and there is high street greenery in the mid-levels and peak, where traditional affluent residential areas are concentrated with more trees. This reason is why the two districts had two peaks of high and low GVF values. The green inequality found in our study is partly consistent with a finding in the literature that the distribution of open space favors upmarket, low-density housing areas in Hong Kong (Tang, 2017).

Twelve new towns have developed since the 1970s and are scattered in the New Territories because of limited urban lands and rising population. They currently accommodate nearly half of the population of Hong Kong (CenStatD, 2018). Street greenery access in new towns is better than that in old urban areas but remains unequal across them. Low street greenery was observed in newly developed towns. The youngest city in Tung Chung, North Lantau, developed in the 1990s, has the highest street greenery, with rapid population growth since the 2000s. This finding suggests that greening has received more attention in the more recent periods in Hong Kong town buildings (Jim & Chan, 2016; Tian et al., 2012).

Regarding land utilization, we found that private residential lands provide less street greenery than public and rural residential lands. The Hong Kong Planning Standards and Guidelines require the provision of a

local open space of at least 1 m^2 per person in public housing and comprehensive residential development (PlanD, 2020a). The requirement results in a certain amount of green space inside housing estates and visible greenery from the streets. Lai (2017) found that in old urban areas in Kowloon or on Hong Kong Island, public housing and large private developments are better provided with open spaces where greenery is generally offered than other private housing, such as small developments and individual buildings. In ultra-high-density Hong Kong, plentiful greenery is legislatively supplied for public housing. However, income and poverty in private housing are easy to ignore. The ignorance further confirms the aforementioned socioeconomic inequality in street greenery provisions. In addition, the low greenery found in commercial and industrial lands and the relatively high greenery found in open spaces in this study were consistent with the findings of a study on Nanjing, China (Tong et al., 2020). Because of the 37,000 GSV points collected and the fine-scale multilevel land use classification in Hong Kong, we could quantify the pedestrian-level greenery in each subcategory of land use.

4.2. Detecting greenery from different perspectives and inconsistency between urban forms

The degrees of street greenery and vegetation cover in the LCZ classes were quantified and found to be consistent with the definitions of LCZs in the quantity of plants. This study may be the first to quantify vegetation in LCZ classes, enriching this knowledge base and providing localized referential evidence for future applications of LCZ classification. The reduced correlation with increasing buffer distance had been observed (Lu et al., 2019; Ye et al., 2019; Yu et al., 2018) and suggests that some distant vegetation captured by the NDVI may not be observed by pedestrians. The overall strong correlation is greater than the estimates in the literature, specifically, moderate correlations separately in Singapore (Ye et al., 2019); Nanjing, China (Tong et al., 2020); and Portland, United States (Larkin & Hystad, 2019), possibly because of the higher proportion of low greenery in Hong Kong's ultra-high-density context. The lower correlation for grids than that for points may result from the vegetation not close to roads being covered by the grid-scale NDVI.

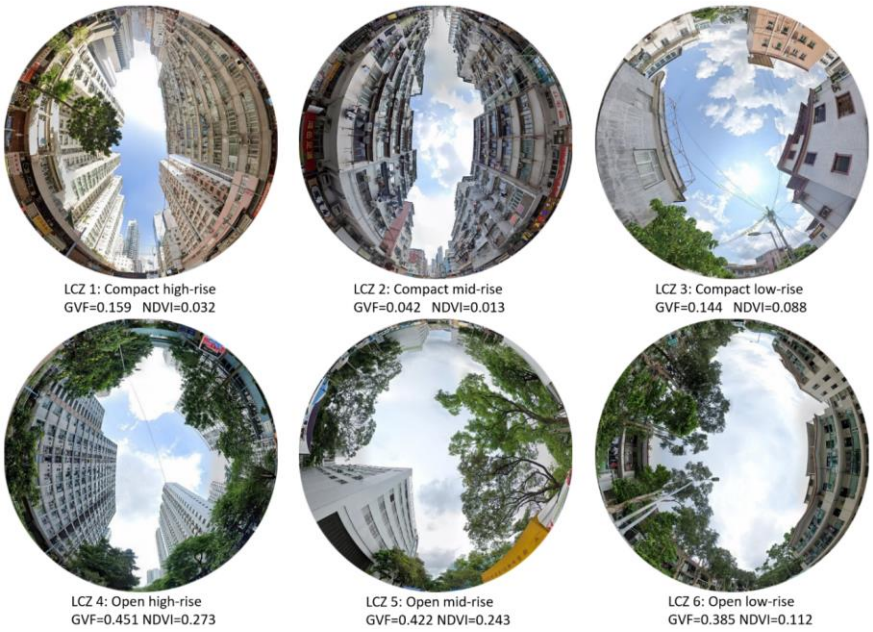

Fig. 11. Sample sites of LCZs 1–6

The inconsistency in correlation across LCZ classes can be attributed to differences in urban morphology. This innovative attempt to adopt LCZ classification as a protocol of urban morphology (Liu et al., 2020) in the investigation of urban greenery provision was assessed from two perspectives. **Error! Reference source not found.** shows the sample sites of LCZs 1–6. In LCZs 1 and 2, the high correlation between the two metrics may be due to the extremely low greenery and difficulties in detecting greenery. In compact, high- and mid-rise areas, satellite sensors cannot identify the greenery well because of blocking by buildings and the steepness of the angle of a satellite sensor (Kumakoshi et al., 2020), although the GVF in a compact high-rise area cannot "see far" and may miss a green park in the next street. Additionally, the NDVI, a product of satellite imagery, is pixel-based and indicates the average status of vegetation within a pixel. In some circumstances, identifying object-based vegetation scattered at street

level is difficult. In LCZs 1 and 2, greenery is likely to be between compact buildings, which may cause a low NDVI because of the non-zero GVF.

Open high- and mid-rise LCZs (4 and 5), widely distributed in the peripheries of old urban areas and within new towns, are featured with more greenery but lower correlations between the two metrics than LCZs 1 and 2. Such open high- or middle-rise contexts have more room for vegetation growth, and greenery at a distance may still be observable because of wider roads and gaps between buildings. This phenomenon enlarges the mismatch between the two perspectives: street views are green because of distant greenery (even mountains in Hong Kong), and earth-view measures only capture local greenery. In this sense, streets in open areas equalize urban morphological features and bring the countryside into urban neighborhoods. The finding will be relevant for public health studies in cities, with wide and open streets functioning not only as movement and ventilation corridors but also as health-giving view corridors (R. Wang et al., 2019; Ruoyu Wang et al., 2019).

Comparatively, low-rise LCZs (3 and 6), mainly distributed in the suburban areas of the New Territories and scattered in the peripheries of urban areas, share lower correlations between the two measurements than high- and mid-rise LCZs (1, 2, 4, and 5). The reasons for this phenomenon are the same as those we have discussed but are more accentuated. In LCZ 6, there is the most space between low-rise buildings for trees with larger canopies to grow, which can be captured well by GSV images when they are far from the street view photography point. The vegetation types (LCZs A–D) were mainly distributed in the margins of urban and suburban areas. In these LCZs, particularly in the dense-tree LCZ, the correlation was significantly lower than that in built-up LCZs because of the extreme divergence of local and distant greenery.

4.3. Inequality in street greenery exposure

Studies on inequalities in green exposure have mainly focused on spatial and demographic variations (Ahn et al., 2020; Kabisch & Haase, 2014), but urban morphology that affects pedestrian-level greenery detection and determines how to improve greenery with the interaction with built environments has been

little considered to address inequalities from a planning perspective. Factors that influence inequality in greenery exposure vary across neighborhoods because of the diverse features of population distribution, street greenery, and urban morphology. Greenery is limited to densely populated areas, which are generally compact. Open areas within or around TPUs can provide accessible greenery. Urban morphology also affects residents' demands. Compact high- and mid-rise areas (LCZs 1 and 2) have high demands from residents for regulating the services of green spaces (Gret-Regamey et al., 2020). Thus, jointly considering the pedestrian-level surrounding greenery measurement, population density, and urban morphology will enable a planning perspective to alleviate environmental injustice in different urban settings in further research.

4.4. Potential implications for urban planning

Hong Kong has committed to improving its urban space by implementing greening master plans (CEDD, 2020), old town renewal, and walkability enhancement measures. All these initiatives require pedestrian-level greenery investigation and creation. The investigation and creation of urban greenery should be implemented from the perspective of end users. Furthermore, in sustainable comminutes and cities, individuals enjoy greenery regardless of residential location and socioeconomic status, highlighting the importance of combining greenery accessibility with population distribution to achieve environmental justice. The GVF measurement describing the green and built environments to which pedestrians are exposed also allows further assessment of ecosystem services provided by greenery for green infrastructure planning (Liu & Russo, 2021).

4.4.1. Implications for greenery investigation and mapping

Greenery planning requires fine-scale mapping of the existing pedestrian-level streetscape greenery. Our case indicates that pedestrian-level greenery in a high-density urban context varies substantially across administrative units and land use types. Therefore, both interactive systems should be considered in urban greenery surveys. Traditional citywide greenery mappings mainly depend on satellite-derived metrics, but in this pioneering study, we found a mismatch between the traditional NDVI and street view-based

measurements and further detected the effect of urban morphology on the mismatch. Because greenery mapping is an initial step for planning, the results from both measurement methods can be complementary but with varying contributions in different urban forms. A higher NDVI does not necessarily mean more greenery exposure for pedestrians in the street. In compact high- and mid-rise areas, where greenery is generally limited, if a very low value of the NDVI is observed, urban planners should be cautious because there may be more or less observable pedestrian-level greenery that cannot be detected at the pixel scale by satellites' overhead view. Comparatively, the GVF is more appropriate for greenery detection in high-density high-rise areas, where street greenery is easier to observe from the ground. In open areas, both measurements were important for greenery mapping. The GVF is less capable of detecting greenery patches behind buildings than NDVI but includes plants that can be observed from the gaps between buildings. The human-perspective measurement by the GSV can help locate areas that not only require but also allow new street greenery.

The difference between the two measures is likely to partially reflect the degree of private gardens. Because the extent of private gardens increases as density decreases, earth-view measures such as the NDVI will continue to increase, limited only by gross residential density, and street view measures will more quickly reach a limit set by the capacity of well-stocked street trees and what can be viewed beyond the street. Another dimension is that in a high-density city, the viewshed from the street is highly curtailed; thus, the green experience from the street is either totally determined by street planting or added to only by the rare bit of green space abutting the street, or perhaps a green mountain glimpsed through a street canyon. For these reasons, the two measures of greenery measure different objects in a very high-density city versus a suburban city. Street view images measure green public goods, which may be the only source of green in some residential areas. Earth-view green picks up the private green supplied by landed condominiums and public parks, and in Hong Kong, the green margins of all built-up areas and the green created by the city's abundant watershed national parks.

4.4.2. Implications to greenery planning and design

More importantly, understanding the mismatch between the two measurements will help in planning and designing pedestrian-oriented greenery in high-density urban contexts. Green coverage is an essential indicator of urban landscaping and can be well reflected by the NDVI. The ultimate objective of urban greening is to improve the city's environment and service citizens. Ground space for new greenery is scarce, particularly in LCZs 1 and 2. Because of the narrow space embraced by compact and tall buildings, one tree or a small amount of vegetation can produce nearby pedestrians with a relatively considerable green view or even serve as a cover from a bottom-up perspective. Existing green spaces require better designs to create visit-friendly spaces that can be easily perceived by people (Xue et al., 2017). Alternative design strategies corrected for buildings, such as green façades, sky gardens, and green pavements (Chàfer et al., 2021). Elevated walkways that facilitate pedestrian shuttling between buildings in high-density areas, such as the central area, are also target places for effective greening. In open areas, trees can be planted in gaps between buildings and mountain views can be introduced to pedestrians through street canyons. Urban parks and pocket gardens can be connected by green tracks to provide diverse paths as alternatives to concrete sidewalks along carriageways. Planting courtyard trees should be promoted in low-rise areas. In compact places, such trees can provide shade, and in open places, they can be enjoyed distantly by pedestrians. Informal green spaces scattered in various places can be identified by street view images and redesigned to provide improved ecosystem services (Włodarczyk-Marciniak et al., 2020). Generally, understanding the effect of urban morphology helps with corresponding greening strategies, particularly in high-density urban contexts.

4.5. Advances and limitations

This study has several advantages. First, it accurately mapped the citywide distribution of pedestrian-level street greenery in a high-density urban context by combining big data from street view images and the deep learning technique. The 50 m interval GSV sampling covered the road network of the entire city of Hong Kong. It provided a large dataset for investigating spatial variations across districts, new towns,

land utilization types, and urban forms. Second, this study introduced the LCZ classification to facilitate a comparison of street view image-based greenery measurements and satellite-derived vegetation indices across different urban forms. The introduction of LCZ permits the development of a new understanding of the differences between two common urban greenery measurements. High spatial resolution data, including 50 m interval citywide street greenery extraction from GSV images, a 10 m resolution NDVI map based on Sentinel-2 satellite images, and a 100 m resolution LCZ map, jointly allow fine-scale mapping of street greenery covering diverse urban forms. Vegetation characteristics across LCZ classes were systematically examined. Third, this study provided a potential procedure to analyze the inequality of street greenery exposure for individuals by considering population data. Finally, this study relied entirely on open data sources, which makes the methods transferrable to other cities.

This study has several limitations. First, although the GSV covers most roads in Hong Kong, areas not covered remain, mainly in suburban areas. In urban areas, some narrow alleys without vehicular access are missed, although greenery is scarce. The internal conditions of large green spaces and greenery inside the boundaries of development cannot be captured by GSV images. Hence, for comprehensive city-level greenery mapping, GSV-based measurements should be integrated with other measurements to capture multiple details of green elements in a high-density urban context. Second, GSV images are mainly taken from the road, but pedestrians use sidewalks. People may be differently exposed to greenery in the case of large roads or those with dramatic differences between the left and right sides. Further research should consider the difference between the two sides of roads and the effect on pedestrian greenery exposure. Another limitation is the inconsistency in the timeframe between the GSV and NDVI data, as mentioned by Larkin and Hystad (2019). In this study, the NDVI was the full-year average value for 2020. Because GSV images are updated from time to time, we included all the data for approximately 37,000 locations for fuller spatial coverage. Among the GSV images collected, approximately 72% were from May to November 2019, and most of the remaining images were taken in the first half of 2020. Although this method ignores the seasonal variation in plant phenology, temporal change may not be significant in

Hong Kong, mainly because in a subtropical climate, most vegetation is evergreen species. Because of a complete mechanism for urban greenery, any changes in urban greenery require rigorous evaluation in Hong Kong; therefore, the changes in urban greenery are typically nonsignificant for a period of one year. Additionally, in 2020, no large-scale city-level COVID-19 lockdown was imposed in Hong Kong; thus, we posit that the spread of COVID-19 did not significantly affect the daily operation of the city. The Hong Kong traffic censuses (TD, 2020, 2021) conducted by the Transport Department showed that road traffic in Hong Kong did not change significantly between 2019 and 2020. Fourth, bivariate spatial autocorrelation is not considered. Bivariate Moran's I (0.64, $p = 0.01$) indicated global spatial autocorrelation. Although GSV images were collected every 50 m along the road network of the city, the central areas, where roads are denser, are more weighted. Bivariate spatial autocorrelation could affect the overall correlation between the GSV and NDVI. In different LCZs, effects may be reduced because each built LCZ class represents a specific urban form with smaller spatial variation. We also identified varying mismatches between the two measurements across the LCZ classes, even if spatial autocorrelation exists; thus, further studies are required to estimate and map the spatial relationships between them. Finally, in the analysis of inequity in greenery, the accessible area of an LCZ grid by walking was simplified to be buffered along the LCZ grid boundary. A realistic accessible area should be located along the pedestrian network. Given that related pedestrian networks have been developed (Sun et al., 2019; Tang et al., 2021), such datasets will allow further research to depict inequity more precisely than it has been in the literature.

5. Conclusions

We developed an indicator, the GVF, to measure pedestrian-level street greenery in a case study of Hong Kong by using GSV images, focusing on estimating the spatial variability of pedestrian-level greenery across the city, comparing pedestrian-level greenery measurements and satellite-derived vegetation metrics in different urban forms, and investigating the inequality of greenery provision.

First, the mean GVF value in Hong Kong is 0.39, and citywide pedestrian-level street greenery in Hong Kong varies across districts, new towns, land utilization types, and urban forms. Old high-density urban

areas, especially those on the Kowloon Peninsula, and land for private residential, commercial, business, and office areas, have notably lower degrees of street greenery. In old urban areas, low street greenery is often associated with low incomes. Regarding urban forms, the study also confirms that open LCZs accommodate more greenery than compact LCZs and finds that compact low-rise areas (LCZ 3) are slightly greener than compact high- and mid-rise areas (LCZs 1 and 2).

Second, pedestrian-level street greenery and remotely sensed vegetation cover, represented by the GVF and NDVI, were strongly correlated overall, but correlations varied across urban forms. The inconsistency between the two measurements increases from high- and mid-rise LCZ classes to low-rise classes, and from compact classes to open classes, and is greater in vegetated areas than in built-up areas. Specifically, the GVF and NDVI were strongly correlated in LCZs 1 and 2 and moderately correlated in LCZs 4 and 5, moderately weakly correlated in LCZs 3 and 6, and weakly correlated in the vegetated areas. Moreover, an extremely low NDVI exists in compact high- and mid-rise areas but does not necessarily mean zero GVF. Thus, this study calls for considering multiple methods to assess urban greenery to establish a holistic view of urban greenery distributions across urban forms and implement corresponding strategies to increase pedestrian-level greenery exposure in different urban forms.

Third, we attempted to integrate surrounding greenery, population density, and urban morphology at a fine scale to demonstrate the potential application of pedestrian-level greenery measurements to address greenery inequality. The surrounding greenery was negatively associated with population density. Neighborhoods vary in aspects, and urban morphology, which affects greenery investigation and creation and resident demands in high-density urban contexts, is key to achieving equity.

The GSV-based greenery indicator developed in this study can reflect the benefits that pedestrians gain from street greenery and innovatively link the detected site-specific street greenery in a high-density urban context with its surrounding urban morphological conditions. In practice, our research findings could help decision-makers and practitioners develop evidence-based urban planning strategies for urban street greening in pursuit of climate-resilient, sustainable, and inclusively healthy cities, such as the

Greening Master Plan in Hong Kong. Methodologically, transferable analytical approaches using open-source data can be applied to other high-density cities with relative ease.

Acknowledgments

The study was supported and funded by the Seed Fund for Basic Research of the University of Hong Kong (Project code: 202011159063).

Declaration of interests

The authors declare that they have no known competing financial interests or personal relationships that could have appeared to influence the work reported in this paper.

References

Ahn, J. J., Kim, Y., Lucio, J., Corley, E. A., & Bentley, M. (2020). Green spaces and heterogeneous social groups in the U.S. *Urban Forestry & Urban Greening, 49*. doi:10.1016/j.ufug.2020.126637

Alshehhi, R., & Marpu, P. R. (2021). Extraction of urban multi-class from high-resolution images using pyramid generative adversarial networks. *International Journal of Applied Earth Observation and Geoinformation, 102*, 102379. doi:https://doi.org/10.1016/j.jag.2021.102379

Åström, D. O., Bertil, F., & Joacim, R. (2011). Heat wave impact on morbidity and mortality in the elderly population: a review of recent studies. *Maturitas, 69*(2), 99-105. doi:10.1016/j.maturitas.2011.03.008

Bartesaghi-Koc, C., Osmond, P., & Peters, A. (2019). Spatio-temporal patterns in green infrastructure as driver of land surface temperature variability: The case of Sydney. *International Journal of Applied Earth Observation and Geoinformation, 83*, 101903. doi:10.1016/j.jag.2019.101903

Bibri, S. E. (2018). A foundational framework for smart sustainable city development: Theoretical, disciplinary, and discursive dimensions and their synergies. *Sustainable Cities and Society, 38*, 758-794. doi:https://doi.org/10.1016/j.scs.2017.12.032

Bondarenko, M., Kerr, D., Sorichetta, A., & Tatem, A. (2020). *Estimates of 2020 total number of people per grid square, adjusted to match the corresponding UNPD 2020 estimates and broken down by gender and age groupings, produced using Built-Settlement Growth Model (BSGM) outputs*.

Breiman, L. (2001). Random Forests. *Machine Learning, 45*(1), 5-32. doi:10.1023/a:1010933404324

Brostow, G. J., Fauqueur, J., & Cipolla, R. (2009). Semantic object classes in video: A high-definition ground truth database. *Pattern Recogn. Lett., 30*(2), 88–97. doi:10.1016/j.patrec.2008.04.005

Carrasco-Hernandez, R., Smedley, A. R. D., & Webb, A. R. (2015). Using urban canyon geometries obtained from Google Street View for atmospheric studies: Potential applications in the calculation of street level total shortwave irradiances. *Energy and Buildings, 86*, 340-348. doi:10.1016/j.enbuild.2014.10.001

CEDD. (2020). Greening Master Plan. Retrieved from https://www.cedd.gov.hk/eng/topics-in-focus/greening/index.html

Chàfer, M., Cabeza, L. F., Pisello, A. L., Tan, C. L., & Wong, N. H. (2021). Trends and gaps in global research of greenery systems through a bibliometric analysis. *Sustainable Cities and Society, 65*, 102608. doi:https://doi.org/10.1016/j.scs.2020.102608

Chen, L.-C., Zhu, Y., Papandreou, G., Schroff, F., & Adam, H. (2018). *Encoder-decoder with atrous separable convolution for semantic image segmentation.* Paper presented at the Proceedings of the European conference on computer vision (ECCV).

Chung, L. C. H., Xie, J., & Ren, C. (2021). Improved machine-learning mapping of local climate zones in metropolitan areas using composite earth observation data in Google Earth Engine. *Building and Environment*, 107879. doi:10.1016/j.buildenv.2021.107879

Cleland, E. E., Chuine, I., Menzel, A., Mooney, H. A., & Schwartz, M. D. (2007). Shifting plant phenology in response to global change. *Trends in Ecology & Evolution, 22*(7), 357-365. doi:10.1016/j.tree.2007.04.003

Davies, R. G., Barbosa, O., Fuller, R. A., Tratalos, J., Burke, N., Lewis, D., . . . Gaston, K. J. (2008). City-wide relationships between green spaces, urban land use and topography. *Urban Ecosystems, 11*(3), 269-287. doi:10.1007/s11252-008-0062-y

Demuzere, M., Hankey, S., Mills, G., Zhang, W., Lu, T., & Bechtel, B. (2020). Combining expert and crowd-sourced training data to map urban form and functions for the continental US. *Scientific Data*, *7*(1), 264. doi:10.1038/s41597-020-00605-z

Dersch, H. (2005). Panorama tools. *World Wide Web*.

Ekkel, E. D., & de Vries, S. (2017). Nearby green space and human health: Evaluating accessibility metrics. *Landscape and Urban Planning, 157*, 214-220. doi:10.1016/j.landurbplan.2016.06.008

Fernandes, C. O., da Silva, I. M., Teixeira, C. P., & Costa, L. (2019). Between tree lovers and tree haters. Drivers of public perception regarding street trees and its implications on the urban green infrastructure planning. *Urban Forestry & Urban Greening, 37*, 97-108. doi:10.1016/j.ufug.2018.03.014

Gong, F.-Y., Zeng, Z.-C., Zhang, F., Li, X., Ng, E., & Norford, L. K. (2018). Mapping sky, tree, and building view factors of street canyons in a high-density urban environment. *Building and Environment, 134*, 155-167. doi:10.1016/j.buildenv.2018.02.042

Gret-Regamey, A., Galleguillos-Torres, M., Dissegna, A., & Weibel, B. (2020). How urban densification influences ecosystem services-a comparison between a temperate and a tropical city. *Environmental Research Letters, 15*(7), 15. doi:10.1088/1748-9326/ab7acf

Haaland, C., & van den Bosch, C. K. (2015). Challenges and strategies for urban green-space planning in cities undergoing densification: A review. *Urban Forestry & Urban Greening, 14*(4), 760-771. doi:10.1016/j.ufug.2015.07.009

Helbich, M., Yao, Y., Liu, Y., Zhang, J. B., Liu, P. H., & Wang, R. Y. (2019). Using deep learning to examine street view green and blue spaces and their associations with geriatric depression in Beijing, China. *Environment International, 126*, 107-117. doi:10.1016/j.envint.2019.02.013

Hesamian, M. H., Jia, W., He, X., & Kennedy, P. (2019). Deep learning techniques for medical image segmentation: Achievements and challenges. *Journal of Digital Imaging, 32*(4), 582-596. doi:10.1007/s10278-019-00227-x

Jiang, B., Deal, B., Pan, H., Larsen, L., Hsieh, C.-H., Chang, C.-Y., & Sullivan, W. C. (2017). Remotely-sensed imagery vs. eye-level photography: Evaluating associations among measurements of tree cover density. *Landscape and Urban Planning, 157*, 270-281. doi:10.1016/j.landurbplan.2016.07.010

Jim, C. Y., & Chan, M. W. H. (2016). Urban greenspace delivery in Hong Kong: Spatial-institutional limitations and solutions. *Urban Forestry & Urban Greening, 18*, 65-85. doi:10.1016/j.ufug.2016.03.015

Kabisch, N., & Haase, D. (2014). Green justice or just green? Provision of urban green spaces in Berlin, Germany. *Landscape and Urban Planning, 122*, 129-139. doi:10.1016/j.landurbplan.2013.11.016

Kabisch, N., van den Bosch, M., & Lafortezza, R. (2017). The health benefits of nature-based solutions to urbanization challenges for children and the elderly - A systematic review. *Environmental Research, 159*, 362-373. doi:10.1016/j.envres.2017.08.004

Kang, Y., Zhang, F., Gao, S., Lin, H., & Liu, Y. (2020). A review of urban physical environment sensing using street view imagery in public health studies. *Annals of GIS, 26*(3), 261-275. doi:10.1080/19475683.2020.1791954

Kumakoshi, Y., Chan, S. Y., Koizumi, H., Li, X., & Yoshimura, Y. (2020). Standardized Green View Index and Quantification of Different Metrics of Urban Green Vegetation. *Sustainability, 12*(18). doi:10.3390/su12187434

Labib, S. M., Lindley, S., & Huck, J. J. (2020). Spatial dimensions of the influence of urban green-blue spaces on human health: A systematic review. *Environmental Research, 180*, 108869. doi:10.1016/j.envres.2019.108869

Lai, C. (2017). *Unopened Space: Mapping Equitable Availability of Open Space in Hong Kong*. Retrieved from Hong Kong: https://civic-exchange.org/wp-content/uploads/2017/04/20170224POSreport_FINAL.pdf

Larkin, A., & Hystad, P. (2019). Evaluating street view exposure measures of visible green space for health research. *Journal of Exposure Science & Environmental Epidemiology, 29*(4), 447-456. doi:10.1038/s41370-018-0017-1

Lau, K. K.-L., Chung, S. C., & Ren, C. (2019). Outdoor thermal comfort in different urban settings of sub-tropical high-density cities: An approach of adopting local climate zone (LCZ) classification. *Building and Environment, 154*, 227-238. doi:10.1016/j.buildenv.2019.03.005

Lehnert, M., Savić, S., Milošević, D., Dunjić, J., & Geletič, J. (2021). Mapping Local Climate Zones and Their Applications in European Urban Environments: A Systematic Literature Review and Future Development Trends. *ISPRS International Journal of Geo-Information, 10*(4). doi:10.3390/ijgi10040260

Li, X. (2020). Examining the spatial distribution and temporal change of the green view index in New York City using Google Street View images and deep learning. *Environment and Planning B: Urban Analytics and City Science*, 2399808320962511. doi:10.1177/2399808320962511

Li, X., Ratti, C., & Seiferling, I. (2018). Quantifying the shade provision of street trees in urban landscape: A case study in Boston, USA, using Google Street View. *Landscape and Urban Planning, 169*, 81-91. doi:10.1016/j.landurbplan.2017.08.011

Li, X., Zhang, C., Li, W., Ricard, R., Meng, Q., & Zhang, W. (2015). Assessing street-level urban greenery using Google Street View and a modified green view index. *Urban Forestry & Urban Greening, 14*(3), 675-685. doi:10.1016/j.ufug.2015.06.006

Liang, J., Gong, J., Zhang, J., Li, Y., Wu, D., & Zhang, G. (2020). GSV2SVF-an interactive GIS tool for sky, tree and building view factor estimation from street view photographs. *Building and Environment, 168*, 106475. doi:10.1016/j.buildenv.2019.106475

Liu, O. Y., & Russo, A. (2021). Assessing the contribution of urban green spaces in green infrastructure strategy planning for urban ecosystem conditions and services. *Sustainable Cities and Society, 68*, 102772. doi:https://doi.org/10.1016/j.scs.2021.102772

Liu, Y., Chen, C., Li, J., & Chen, W.-Q. (2020). Characterizing three dimensional (3-D) morphology of residential buildings by landscape metrics. *Landscape Ecology, 35*(11), 2587-2599. doi:10.1007/s10980-020-01084-8

Lu, Y. (2018). The Association of Urban Greenness and Walking Behavior: Using Google Street View and Deep Learning Techniques to Estimate Residents' Exposure to Urban Greenness. *International Journal of Environmental Research and Public Health, 15*(8), 1576. doi:10.3390/ijerph15081576

Lu, Y. (2019). Using Google Street View to investigate the association between street greenery and physical activity. *Landscape and Urban Planning, 191*. doi:10.1016/j.landurbplan.2018.08.029

Lu, Y., Yang, Y. Y., Sun, G. B., & Gou, Z. H. (2019). Associations between overhead-view and eye-level urban greenness and cycling behaviors. *Cities, 88*, 10-18. doi:10.1016/j.cities.2019.01.003

MacFaden, S., O'Neil-Dunne, J. P., Royar, A., Lu, J. W., & Rundle, A. (2012). High-resolution tree canopy mapping for New York City using LIDAR and object-based image analysis. *Journal of Applied Remote Sensing, 6*(1), 063567. doi:10.1117/1.JRS.6.063567

Middel, A., Lukasczyk, J., Maciejewski, R., Demuzere, M., & Roth, M. (2018). Sky View Factor footprints for urban climate modeling. *Urban Climate, 25*, 120-134. doi:10.1016/j.uclim.2018.05.004

Middel, A., Lukasczyk, J., Zakrzewski, S., Arnold, M., & Maciejewski, R. (2019). Urban form and composition of street canyons: A human-centric big data and deep learning approach. *Landscape and Urban Planning, 183*, 122-132. doi:10.1016/j.landurbplan.2018.12.001

Mullaney, J., Lucke, T., & Trueman, S. J. (2015). A review of benefits and challenges in growing street trees in paved urban environments. *Landscape and Urban Planning, 134*, 157-166. doi:10.1016/j.landurbplan.2014.10.013

Neuhold, G., Ollmann, T., Rota Bulo, S., & Kontschieder, P. (2017). *The mapillary vistas dataset for semantic understanding of street scenes.* Paper presented at the Proceedings of the IEEE international conference on computer vision.

Oke, T. R. (1981). Canyon geometry and the nocturnal urban heat island: Comparison of scale model and field observations. *Journal of Climatology, 1*(3), 237-254. doi:10.1002/joc.3370010304

Pal, M. (2005). Random forest classifier for remote sensing classification. *International Journal of Remote Sensing, 26*(1), 217-222. doi:10.1080/01431160412331269698

Pettorelli, N., Vik, J. O., Mysterud, A., Gaillard, J.-M., Tucker, C. J., & Stenseth, N. C. (2005). Using the satellite-derived NDVI to assess ecological responses to environmental change. *Trends in Ecology & Evolution, 20*(9), 503-510. doi:10.1016/j.tree.2005.05.011

Pham, T.-T.-H., Apparicio, P., Landry, S., & Lewnard, J. (2017). Disentangling the effects of urban form and socio-demographic context on street tree cover: A multi-level analysis from Montréal. *Landscape and Urban Planning, 157*, 422-433. doi:10.1016/j.landurbplan.2016.09.001

PlanD. (2016a). *Hong Kong 2030+: Planning and Urban Design for a Liveable High-Density City*. Retrieved from https://www.hk2030plus.hk/document/Planning%20and%20Urban%20Design%20for%20a%20Liveable%20High-Density%20City_Eng.pdf

PlanD. (2020a). *Chapter 4 Recreation, Open Space and Greening*. Planning Department, HKSAR Government Retrieved from https://www.pland.gov.hk/pland_en/tech_doc/hkpsg/full/pdf/ch4.pdf

PlanD. (2020b). Land Utilization in Hong Kong 2019. Retrieved from https://www.pland.gov.hk/pland_en/info_serv/statistic/landu.html

PlanD. (2021). *Chapter 8 Internal Transport Facilities*. Planning Department, HKSAR Government Retrieved from https://www.pland.gov.hk/pland_en/tech_doc/hkpsg/full/pdf/ch8.pdf

Richards, D. R., & Edwards, P. J. (2017). Quantifying street tree regulating ecosystem services using Google Street View. *Ecological Indicators, 77*, 31-40. doi:10.1016/j.ecolind.2017.01.028

Roy, S., Byrne, J., & Pickering, C. (2012). A systematic quantitative review of urban tree benefits, costs, and assessment methods across cities in different climatic zones. *Urban Forestry & Urban Greening, 11*(4), 351-363. doi:https://doi.org/10.1016/j.ufug.2012.06.006

Rundle, A. G., Bader, M. D. M., Richards, C. A., Neckerman, K. M., & Teitler, J. O. (2011). Using Google Street View to Audit Neighborhood Environments. *American Journal of Preventive Medicine, 40*(1), 94-100. doi:10.1016/j.amepre.2010.09.034

Seiferling, I., Naik, N., Ratti, C., & Proulx, R. (2017). Green streets − Quantifying and mapping urban trees with street-level imagery and computer vision. *Landscape and Urban Planning, 165*, 93-101. doi:10.1016/j.landurbplan.2017.05.010

Shahtahmassebi, A. R., Li, C., Fan, Y., Wu, Y., lin, Y., Gan, M., . . . Blackburn, G. A. (2021). Remote sensing of urban green spaces: A review. *Urban Forestry & Urban Greening, 57*. doi:10.1016/j.ufug.2020.126946

Siam, M., Elkerdawy, S., Jagersand, M., & Yogamani, S. (2017). *Deep semantic segmentation for automated driving: Taxonomy, roadmap and challenges.* Paper presented at the 2017 IEEE 20th international conference on intelligent transportation systems (ITSC).

Stewart, I. D., & Oke, T. R. (2012). Local Climate Zones for Urban Temperature Studies. *Bulletin of the American Meteorological Society, 93*(12), 1879-1900. doi:10.1175/bams-d-11-00019.1

Steyn, D. G. (1980). The calculation of view factors from fisheye- lens photographs: Research note. *Atmosphere-Ocean, 18*(3), 254-258. doi:10.1080/07055900.1980.9649091

Sun, G., Webster, C., & Zhang, X. (2019). Connecting the city: A three-dimensional pedestrian network of Hong Kong. *Environment and Planning B: Urban Analytics and City Science, 48*(1), 60-75. doi:10.1177/2399808319847204

Tang, B.-s. (2017). Is the distribution of public open space in Hong Kong equitable, why not? *Landscape and Urban Planning, 161*, 80-89. doi:10.1016/j.landurbplan.2017.01.004

Tang, B.-S., Wong, K. K. H., Tang, K. S. S., & Wai Wong, S. (2021). Walking accessibility to neighbourhood open space in a multi-level urban environment of Hong Kong. *Environment and Planning B: Urban Analytics and City Science, 48*(5), 1340-1356. doi:10.1177/2399808320932575

TD. (2020). *Annual Traffic Census 2019*. Transport Department Retrieved from https://www.td.gov.hk/filemanager/en/content_5018/annual%20traffic%20census%202019.pdf

TD. (2021). *Annual Traffic Census 2020*. Transport Department Retrieved from https://www.td.gov.hk/filemanager/en/content_5114/annual%20traffic%20census%202020.pdf

Tian, Y., Jim, C. Y., & Tao, Y. (2012). Challenges and Strategies for Greening the Compact City of Hong Kong. *Journal of Urban Planning and Development, 138*(2), 101-109. doi:10.1061/(asce)up.1943-5444.0000076

Tong, M., She, J., Tan, J., Li, M., Ge, R., & Gao, Y. (2020). Evaluating Street Greenery by Multiple Indicators Using Street-Level Imagery and Satellite Images: A Case Study in Nanjing, China. *Forests, 11*(12). doi:10.3390/f11121347

Turner-Skoff, J. B., & Cavender, N. (2019). The benefits of trees for livable and sustainable communities. *PLANTS, PEOPLE, PLANET, 1*(4), 323-335. doi:https://doi.org/10.1002/ppp3.39

Villeneuve, P. J., Ysseldyk, R. L., Root, A., Ambrose, S., DiMuzio, J., Kumar, N., . . . Rainham, D. (2018). Comparing the Normalized Difference Vegetation Index with the Google Street View Measure of Vegetation to Assess Associations between Greenness, Walkability, Recreational Physical Activity, and Health in Ottawa, Canada. *International Journal of Environmental Research and Public Health, 15*(8). doi:10.3390/ijerph15081719

Wang, R., Helbich, M., Yao, Y., Zhang, J., Liu, P., Yuan, Y., & Liu, Y. (2019). Urban greenery and mental wellbeing in adults: Cross-sectional mediation analyses on multiple pathways across different greenery measures. *Environmental Research, 176*, 108535. doi:10.1016/j.envres.2019.108535

Wang, R., Lu, Y., Zhang, J., Liu, P., Yao, Y., & Liu, Y. (2019). The relationship between visual enclosure for neighbourhood street walkability and elders' mental health in China: Using street view images. *Journal of Transport & Health, 13*, 90-102. doi:10.1016/j.jth.2019.02.009

Włodarczyk-Marciniak, R., Sikorska, D., & Krauze, K. (2020). Residents' awareness of the role of informal green spaces in a post-industrial city, with a focus on regulating services and urban adaptation potential. *Sustainable Cities and Society, 59*, 102236. doi:https://doi.org/10.1016/j.scs.2020.102236

Wolch, J. R., Byrne, J., & Newell, J. P. (2014). Urban green space, public health, and environmental justice: The challenge of making cities 'just green enough'. *Landscape and Urban Planning, 125*, 234-244. doi:10.1016/j.landurbplan.2014.01.017

Xu, Y., Ren, C., Ma, P., Ho, J., Wang, W., Lau, K. K.-L., . . . Ng, E. (2017). Urban morphology detection and computation for urban climate research. *Landscape and Urban Planning, 167*, 212-224. doi:10.1016/j.landurbplan.2017.06.018

Xue, F., Gou, Z., & Lau, S. S. Y. (2017). Green open space in high-dense Asian cities: Site configurations, microclimates and users' perceptions. *Sustainable Cities and Society, 34*, 114-125. doi:10.1016/j.scs.2017.06.014

Xue, J., You, R., Liu, W., Chen, C., & Lai, D. (2020). Applications of Local Climate Zone Classification Scheme to Improve Urban Sustainability: A Bibliometric Review. *Sustainability, 12*(19). doi:10.3390/su12198083

Yang, J., Zhao, L., McBride, J., & Gong, P. (2009). Can you see green? Assessing the visibility of urban forests in cities. *Landscape and Urban Planning, 91*(2), 97-104. doi:10.1016/j.landurbplan.2008.12.004

Yang, Y., Tang, R., Qiu, H., Lai, P. C., Wong, P., Thach, T. Q., . . . Barratt, B. (2018). Long term exposure to air pollution and mortality in an elderly cohort in Hong Kong. *Environment International, 117*, 99-106. doi:10.1016/j.envint.2018.04.034

Ye, Y., Richards, D., Lu, Y., Song, X., Zhuang, Y., Zeng, W., & Zhong, T. (2019). Measuring daily accessed street greenery: A human-scale approach for informing better urban planning practices. *Landscape and Urban Planning, 191*. doi:10.1016/j.landurbplan.2018.08.028

Yu, X., Zhao, G., Chang, C., Yuan, X., & Heng, F. (2018). BGVI: A New Index to Estimate Street-Side Greenery Using Baidu Street View Image. *Forests, 10*(1). doi:10.3390/f10010003

Zhang, J., Yu, Z., Cheng, Y., Chen, C., Wan, Y., Zhao, B., & Vejre, H. (2020). Evaluating the disparities in urban green space provision in communities with diverse built environments: The case of a rapidly urbanizing Chinese city. *Building and Environment, 183*. doi:10.1016/j.buildenv.2020.107170

Zhao, C., Weng, Q., & Hersperger, A. M. (2020). Characterizing the 3-D urban morphology transformation to understand urban-form dynamics: A case study of Austin, Texas, USA. *Landscape and Urban Planning, 203*. doi:10.1016/j.landurbplan.2020.103881

Zheng, Y., Ren, C., Xu, Y., Wang, R., Ho, J., Lau, K., & Ng, E. (2018). GIS-based mapping of Local Climate Zone in the high-density city of Hong Kong. *Urban Climate, 24*, 419-448. doi:10.1016/j.uclim.2017.05.008

Supplementary Material

Methods

1. GSV data collection

A set of points of interest were collected by extracting geolocation (latitude and longitude) along each street. Each location with available GSV panoramas corresponds to a panorama ID, which can be acquired by matching the geolocation of the nearest point of interest. With the panorama ID, each street view image can be requested by defining parameters in the HTTP URL form at https://maps.googleapis.com/maps/api/streetview?parameters via the Street View Static API. To generate a complete street view panorama, we made multiple requests for each location and sent in the form of HTTP URLs by varying the heading (compass heading of the camera), horizontal field of view of the image, and pitch (vertical angle of the camera). Over 400,000 GSV images at 53,000 locations were collected by sending requests via the GSV Image API.

2. Greenery extraction using deep learning and validation

Recently developed deep learning techniques have allowed a more accurate detection of vegetation from street view images. Different from unsupervised classification methods based on the natural colors of the images, exampled by Li et al. (2015), deep-learning algorithms are more able to extract vegetation distinct from other features such as sky, roads, and buildings with higher accuracies and less misidentification of green objects that are not vegetation (Gong et al., 2018; Helbich et al., 2019; Li, 2020; Lu, 2018; Ye et al., 2019). Moreover, deep learning further underlines the advantages of street view-based measurements in automatic, and batch processing.

Semantic segmentation with deep learning has been proved effective in pattern recognition and is a state-of-the-art and powerful tool to extract information from images (Hesamian et al., 2019). We applied the deep learning technique to the 37,000 panorama images for the extraction of greenery information. Semantic segmentation of images generally contains three steps: first, annotated images with labels are

used to train a segmentation network; second, new images are fed into the pre-trained network for segmentation; finally, the segmentation results are evaluated by comparing predicted labels with ground-truth labels.

A large amount of annotated image datasets is fundamental to the semantic segmentation with deep learning, and the recent development of annotated image databases has significantly sped up the semantic segmentation process (Siam et al., 2017). In this study, we applied a pre-trained network generated from the Cambridge-driving Labeled Video Database (CamVid) (Brostow et al., 2009) and the Deeplab v3+ network (Chen et al., 2018) with weights initialized from a pre-trained Resnet-18 network (Alshehhi & Marpu, 2021). The CamVid contains street view images with pixel-level ground-truth labels for 32 semantic classes such as vegetation, sky, building, pedestrian, car, and road. Each pixel in the frames of the CamVid dataset is manually labeled with a class by volunteers and examined by another person. It has been found that CamVid has the accuracy of 96% for the road category and an overall accuracy of 75% for all 11 classes (Brostow et al., 2009). Therefore, the CamVid dataset is suitable for this study because of the sufficient annotation of street objects and the precise labelling. We used the ResNet-18 for its outstanding balance between accuracy and efficiency, and it has been examined for vegetation identification (Xiang et al., 2021). The pre-trained network was applied to the 37,000 panorama images to classify objects into the predefined 32 classes, which were further categorized into three main classes, i.e., vegetation, urban, and sky. The vegetation class captures all vegetation including trees and other greenery, while the urban class covers objects except greenery and sky. Finally, 50 panorama images were randomly chosen out of the 37,000 panorama images and were applied to validate the segmentation results. The selected images were manually labeled with the three classes as independent ground-truth and cross-compared with the corresponding segmentation image. The accuracy can be quantified using a confusion matrix. The accuracy of the vegetation class was up to 95%.

3. Normalized Difference Vegetation Index

NDVI captures vegetation health on the basis of light reflectance (Cleland et al., 2007; Pettorelli et al., 2005). Space-borne European Space Agency Sentinel-2 MSI Level-2A imagery is suitable for calculating NDVI, from Band 4 - Red (665 nm) and Band 8 - NIR (842 nm), with a 10-meter spatial resolution at the landscape-level observations. In the GEE platform, cloud-free pixels were selected to compute the NDVI values of each obtained date of Sentinel-2 using the following equation:

$$NDVI = (NIR - Red)/(NIR + Red).$$

Tables

Table S1 Local climate zones (LCZs) and its simplified surface properties (Stewart & Oke, 2012)

LCZ types	Built and land cover types	Anthropogenic heat flux density[f]	Aspect ratio[a]	Sky view factor[b]	Building surface fraction[c]	Impervious surface fraction[d]	Height of roughness elements[e]
LCZ 1	Compact high-rise	50–300	>2	0.2–0.4	40–60	40–60	>25
LCZ 2	Compact mid-rise	<75	0.75–1.5	0.3–0.6	40–70	30–50	8–20
LCZ 3	Compact low-rise	<75	0.75–1.5	0.2–0.6	40–70	20–40	3–8
LCZ 4	Open high-rise	<50	0.75–1.25	0.5–0.7	20–40	30–40	>25
LCZ 5	Open mid-rise	<25	0.3–0.75	0.5–0.8	20–40	30–50	8–20
LCZ 6	Open low-rise	<25	0.3–0.75	0.6–0.9	20–40	20–40	3–8
LCZ 7	Lightweight low-rise	<35	1–2	0.2– 0.5	60–90	<10	2–4
LCZ 8	Large low-rise	<50	0.1–0.3	>0.7	30–50	40–50	3–10
LCZ 9	Sparsely built	<10	0.1–0.25	>0.8	10–20	<20	3–8
LCZ 10	Heavy industry	>300	0.2–0.5	0.6–0.9	20–30	20–40	5–15
LCZ A	Dense trees	0	>1	<0.4	<10	<10	3–30
LCZ B	Scattered trees	0	0.25–0.75	0.5–0.8	<10	<10	3–15
LCZ C	Bush, scrub	0	0.25–1.0	>0.9	<10	<10	<2
LCZ D	Low plants	0	<0.1	>0.9	<10	<10	<1
LCZ E	Bare rock or paved	0	<0.1	>0.9	<10	>90	<0.25
LCZ F	Bare soil or sand	0	<0.1	>0.9	<10	<10	<0.25
LCZ G	Water	0	<0.1	>0.9	<10	<10	—
LCZ H	Wetlands	0	<0.1	>0.9	<10	<10	—

[a]Mean height-to-width ratio of street canyons (LCZs 1–7), building spacing (LCZs 8–10), and tree spacing (LCZs A–G).
[b]Ratio of the amount of sky hemisphere visible from ground level to that for an unobstructed hemisphere.
[c]Proportion of ground surface with building cover (%).
[d]Proportion of ground surface with impervious cover (rock, paved) (%).
[e]Geometric average of building heights (LCZs 1–10) and tree/plant heights (LCZs A–F) (m).
[f]Mean annual anthropogenic heat flux density (Wm−2) at the local scale. It varies significantly with latitude, season, and population density.
[g]Wetlands is an additional LCZ type that adapted the land surface properties of coastal cities in the study areas.

Table S2 Complete confusion matrix of Random Forest with the highest overall accuracy in the SS classifier scenario developed by Chung et al. (2021)

LCZ	1	2	3	4	5	6	7	8	9	10	A	B	C	D	E	F	G	H	No. Classified Pixels	User Accuracy (%)
1	429	41	19	57	20	1	6	0	4	15	0	3	0	1	3	1	0	0	600	71.50
2	99	350	77	9	14	8	5	0	0	31	0	3	0	2	1	1	0	0	600	58.33
3	7	37	475	6	8	6	29	1	1	24	0	0	0	6	0	0	0	0	600	79.17
4	40	15	9	497	15	9	0	0	0	13	0	0	0	0	0	2	0	0	600	82.83
5	48	17	10	43	405	54	11	0	5	0	4	1	0	0	0	2	0	0	600	67.50
6	3	9	3	2	17	527	4	1	7	15	0	7	0	0	3	2	0	0	600	87.83
7	1	8	79	0	2	2	502	0	0	0	0	0	0	5	0	0	0	1	600	83.67
8	3	1	10	4	3	0	0	516	0	46	0	0	0	1	15	1	0	0	600	86.00
9	3	8	4	12	23	14	3	1	435	28	14	9	19	8	5	14	0	0	600	72.50
10	1	7	25	3	3	0	0	1	0	514	0	0	0	1	38	6	0	1	600	85.67
A	0	0	0	2	0	5	0	0	15	0	510	40	25	1	0	0	0	2	600	85.00
B	1	2	1	33	1	19	1	0	14	9	122	304	58	15	1	17	0	2	600	50.67
C	0	0	1	0	0	4	3	0	30	3	22	75	361	9	0	92	0	0	600	60.17
D	0	0	0	0	2	0	2	0	0	0	25	5	10	531	2	7	0	16	600	88.50
E	0	4	7	6	1	0	4	16	3	30	0	0	0	27	472	28	0	2	600	78.67
F	2	0	13	14	5	6	3	26	3	33	0	1	30	77	91	293	0	3	600	48.83
G	0	0	1	0	0	0	0	0	0	1	0	0	0	1	1	0	593	3	600	98.83
H	0	0	0	0	0	1	8	0	0	0	0	0	0	30	0	2	59	500	600	83.33
No. Ground Truth Pixels	637	499	734	688	519	656	581	562	517	762	697	448	503	715	632	468	652	530	10800	
Producer Accuracy (%)	67.35	70.14	64.71	72.24	78.03	80.34	86.40	91.81	84.14	67.45	73.17	67.86	71.77	74.27	74.68	62.61	90.95	94.34		
Overall Accuracy	76.06%		**Built Accuracy**		73.40%			**Land Coverings Accuracy**			71.57%									
Kappa	0.7465																			

For LCZ classification assessment, a confusion matrix was generated to assess the training and expected accuracy of LCZ types. The Producer Accuracy is the training accuracy generated by the classification model on the LCZ training samples. It presents how well the performance of the Random Forest classifier is in recognizing the training samples after learning from the same input dataset. The User Accuracy is the expected accuracy created by the classification model on the validation LCZ samples. It shows the performance of the Random Forest classifier in classifying unknown input data from known LCZ training samples.

Formatted: Font: (Default) Times New Roman, 11 pt, (Asian) Chinese (PRC), (Other) English (United States)

Formatted: Normal, Justified

Formatted: Font: (Asian) Chinese (PRC)

Table S3 Results of the Wilcoxon rank-sum tests

	GVF				NDVI			
	Point scale		Grid scale		Point scale		Grid scale	
	Z	p	Z	p	Z	p	Z	p
Compact (LCZs 1–3) / Open (LCZs 4–6)	84.876	0.0001	62.078	0.0001	99.783	0.0001	79.483	0.0001
Low (LCZs 3,6) / High- and mid-rise (LCZs 1,2,4,5)	8.587	0.0001	5.777	0.0001	18.624	0.0001	10.758	0.0001
Built types (LCZs 1–10) / Vegetated types (LCZs A–D)	74.870	0.0001	57.247	0.0001	93.370	0.0001	73.195	0.0001

We used Wilcoxon rank sum tests to compare GVF and NDVI between groups of points and grids in terms of compactness, height, and land cover. There are statistically significant differences between compact LCZs (1–3) and open LCZs (4–6), between low-rise LCZs (3 & 6) and high- and mid-rise LCZs (1, 2, 4, & 5), and between built types (LCZs 1–10) and vegetated LCZs (A–D) for both grid and point data series of GVF and NDVI.

Formatted: Font: (Asian) Chinese (PRC)

Figures

Fig. S1. Local climate zone classification Demuzere et al. (2020) (derived from https://www.wudapt.org/lcz-resources/)

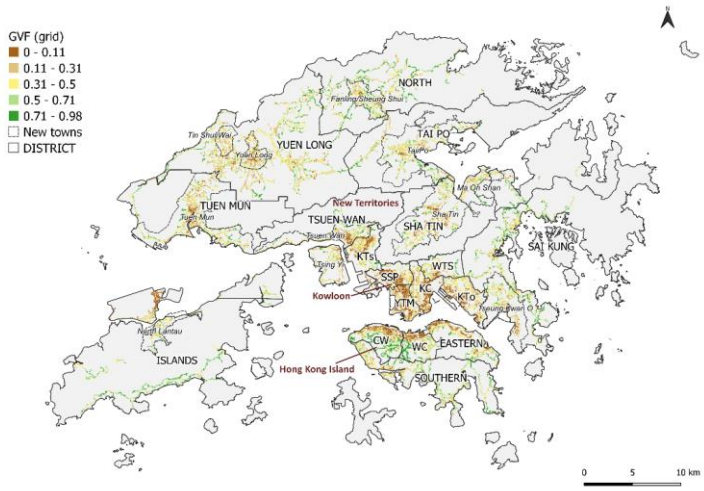

Fig. S2 Map of LCZ grid-based GVF of the whole city

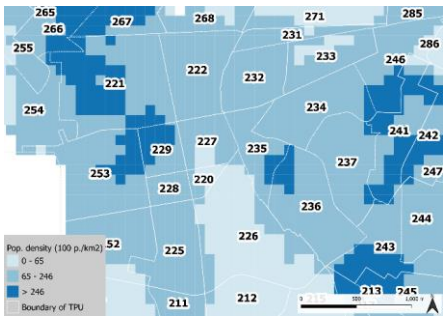

Fig. S3 Elderly population density in Kowloon Peninsula

References

Alshehhi, R., & Marpu, P. R. (2021). Extraction of urban multi-class from high-resolution images using pyramid generative adversarial networks. International Journal of Applied Earth Observation and Geoinformation, 102, 102379. doi:https://doi.org/10.1016/j.jag.2021.102379

Brostow, G. J., Fauqueur, J., & Cipolla, R. (2009). Semantic object classes in video: A high-definition ground truth database. Pattern Recogn. Lett., 30(2), 88–97. doi:10.1016/j.patrec.2008.04.005

Chen, L.-C., Zhu, Y., Papandreou, G., Schroff, F., & Adam, H. (2018). Encoder-decoder with atrous separable convolution for semantic image segmentation. Paper presented at the Proceedings of the European conference on computer vision (ECCV).

Chung, L. C. H., Xie, J., & Ren, C. (2021). Improved machine-learning mapping of local climate zones in metropolitan areas using composite earth observation data in Google Earth Engine. Building and Environment, 107879. doi:10.1016/j.buildenv.2021.107879

Cleland, E. E., Chuine, I., Menzel, A., Mooney, H. A., & Schwartz, M. D. (2007). Shifting plant phenology in response to global change. Trends in Ecology & Evolution, 22(7), 357-365. doi:10.1016/j.tree.2007.04.003

Demuzere, M., Hankey, S., Mills, G., Zhang, W., Lu, T., & Bechtel, B. (2020). Combining expert and crowd-sourced training data to map urban form and functions for the continental US. Scientific Data, 7(1), 264. doi:10.1038/s41597-020-00605-z

Gong, F.-Y., Zeng, Z.-C., Zhang, F., Li, X., Ng, E., & Norford, L. K. (2018). Mapping sky, tree, and building view factors of street canyons in a high-density urban environment. Building and Environment, 134, 155-167. doi:10.1016/j.buildenv.2018.02.042

Helbich, M., Yao, Y., Liu, Y., Zhang, J. B., Liu, P. H., & Wang, R. Y. (2019). Using deep learning to examine street view green and blue spaces and their associations with geriatric depression in Beijing, China. Environment International, 126, 107-117. doi:10.1016/j.envint.2019.02.013

Hesamian, M. H., Jia, W., He, X., & Kennedy, P. (2019). Deep learning techniques for medical image segmentation: Achievements and challenges. Journal of Digital Imaging, 32(4), 582-596. doi:10.1007/s10278-019-00227-x

Li, X. (2020). Examining the spatial distribution and temporal change of the green view index in New York City using Google Street View images and deep learning. Environment and Planning B: Urban Analytics and City Science, 2399808320962511. doi:10.1177/2399808320962511

Li, X., Zhang, C., Li, W., Ricard, R., Meng, Q., & Zhang, W. (2015). Assessing street-level urban greenery using Google Street View and a modified green view index. Urban Forestry & Urban Greening, 14(3), 675-685. doi:10.1016/j.ufug.2015.06.006

Lu, Y. (2018). The Association of Urban Greenness and Walking Behavior: Using Google Street View and Deep Learning Techniques to Estimate Residents' Exposure to Urban Greenness. International Journal of Environmental Research and Public Health, 15(8), 1576. doi:10.3390/ijerph15081576

Pettorelli, N., Vik, J. O., Mysterud, A., Gaillard, J.-M., Tucker, C. J., & Stenseth, N. C. (2005). Using the satellite-derived NDVI to assess ecological responses to environmental change. Trends in Ecology & Evolution, 20(9), 503-510. doi:10.1016/j.tree.2005.05.011

Siam, M., Elkerdawy, S., Jagersand, M., & Yogamani, S. (2017). Deep semantic segmentation for automated driving: Taxonomy, roadmap and challenges. Paper presented at the 2017 IEEE 20th international conference on intelligent transportation systems (ITSC).

Stewart, I. D., & Oke, T. R. (2012). Local Climate Zones for Urban Temperature Studies. Bulletin of the American Meteorological Society, 93(12), 1879-1900. doi:10.1175/bams-d-11-00019.1

Xiang, L., Cai, M., Ren, C., & Ng, E. (2021). Modeling pedestrian emotion in high-density cities using visual exposure and machine learning: Tracking real-time physiology and psychology in Hong Kong. Building and Environment, 205. doi:10.1016/j.buildenv.2021.108273

Ye, Y., Richards, D., Lu, Y., Song, X., Zhuang, Y., Zeng, W., & Zhong, T. (2019). Measuring daily accessed street greenery: A human-scale approach for informing better urban planning practices. Landscape and Urban Planning, 191. doi:10.1016/j.landurbplan.2018.08.028